NASA TECHNICAL NOTE

NASA TN D-3383

NASA TN D-3383

NUMERICAL SOLUTIONS FOR BLUNT AXISYMMETRIC BODIES IN A SUPERSONIC SPHERICAL SOURCE FLOW

by Mamoru Inouye

Ames Research Center

Moffett Field, Calif.

NATIONAL AERONAUTICS AND SPACE ADMINISTRATION • WASHINGTON, D. C. • APRIL 1966

NASA TN D-3383

NUMERICAL SOLUTIONS FOR BLUNT AXISYMMETRIC BODIES IN A SUPERSONIC SPHERICAL SOURCE FLOW

By Mamoru Inouye

Ames Research Center
Moffett Field, Calif.

NATIONAL AERONAUTICS AND SPACE ADMINISTRATION

For sale by the Clearinghouse for Federal Scientific and Technical Information
Springfield, Virginia 22151 – Price $0.55

NUMERICAL SOLUTIONS FOR BLUNT AXISYMMETRIC BODIES IN A SUPERSONIC SPHERICAL SOURCE FLOW

By Mamoru Inouye
Ames Research Center

SUMMARY

The effect of spherical source flow about blunt-nosed axisymmetric bodies has been studied by solving numerically the inviscid equations of motion. An inverse method is used in the subsonic-transonic region, and the method of characteristics is used in the supersonic region. The fluid may be a perfect gas or a real gas in thermodynamic equilibrium.

Solutions have been obtained for spherical-nosed bodies in perfect gas flow to demonstrate the effects of source flow in terms of a parameter defined as the ratio of the nose radius of curvature to the distance between the nose and source. In the nose region, the increase in stagnation-point velocity gradient and decrease in shock standoff distance and surface pressure away from the stagnation point are of the same order of magnitude as the source flow parameter. Over the afterbody of a hemisphere cylinder and a blunted 15° cone, the reductions in surface pressure and outward displacement of the shock are an order of magnitude larger than the source flow parameter. For a blunted 30° cone, the reductions in surface pressure are similarly significant, but the changes in the shock configuration are small.

Results from the present calculation method are compared with predictions of approximate theories and methods in order to evaluate their usefulness. In addition, comparisons have been made with experimental results obtained from tests conducted in conical nozzles.

Author

INTRODUCTION

Some high-speed experimentation is unavoidably carried out in facilities with nonuniform free-stream conditions. Notably, the use of conical nozzles in wind tunnels results in axial gradients of flow properties and finite stream angles away from the axis. The effect of these nonuniformities on the flow around blunt-nosed bodies is naturally of great interest. For example, the size of the test model is limited by the severity of the free-stream gradients. Alternatively, the experimental results could be corrected for the effects of the nonuniform stream.

The methods used in the past to study source flow over blunt bodies have been approximate. For the stagnation region Berndt (ref. 1) used the constant-density approximation to show the effect of source flow on the shock standoff distance and stagnation-point velocity gradient. For the aft portion of blunted slender bodies, Hall (ref. 2) assumed a source flow had effects on

surface pressure and shock-wave shape that could be expressed as small perturbations of the uniform flow values. Baradell and Bertram (ref. 3) used the method of characteristics with nonuniform free-stream conditions ahead of the shock; however, lacking a general solution for the subsonic region, the nose shape was restricted to a sonic wedge or cone. Eaves and Lewis (ref. 4) circumvented this problem by assuming negligible effect of source flow on the subsonic-transonic region and thereby permitting the use of a uniform flow blunt-body solution as input for the method of characteristics. A more complete list of references can be found in Hall (ref. 2).

Computer programs developed at Ames Research Center to calculate the flow field around blunt-nosed bodies in a uniform free stream are described in reference 5. These programs solve numerically the exact equations of motion for plane or axisymmetric inviscid flow of a perfect gas or a real gas in thermodynamic equilibrium. Although the use of these programs restricts the type of problems that can be studied, the solutions are as exact as possible with a numerical method. It is possible to modify these programs to account for a nonuniform free stream, provided the conditions of symmetry are maintained; that is, both the body and free stream must be either plane or axisymmetric. An arbitrary variation of free-stream properties along and normal to the axis may be prescribed consistent with the conditions of mass conservation and isentropic flow. Since conical nozzles are of most interest, the present study will be restricted to axisymmetric bodies in a spherical source flow.

The purpose of the present report is to describe the calculation method used to study spherical source flow around blunt-nosed bodies of revolution and to present results for perfect gas flow that demonstrate the effects on shock-wave shape, standoff distance, stagnation-point velocity gradient, and surface-pressure distribution. Comparisons are made with predictions of approximate methods in order to assess their usefulness. Comparisons are also made with pressure distributions measured on models tested in conical nozzles including real gas effects. The present results may be used as a guide in applying the calculation method to specific cases of flow conditions and model geometry.

SYMBOLS

A_7 shock-wave shape parameter (see eq. (1))

B_b ellipsoid bluntness, $\left(\frac{b}{c}\right)^2$

b,c semiaxes of ellipsoid (see fig. 7)

C_1,C_2,C_3 shock-wave shape parameters (see eq. (2))

C_D drag coefficient, $\frac{D}{(1/2)\rho_o V_o^2 \pi R_b^2}$

D	drag force
L	distance between source and point on bow wave
L_o	distance between source and stagnation point on body
M	Mach number
p	pressure
R_b	radius of curvature of the body at the stagnation point
R_s	radius of curvature of the shock wave for $y = 0$
s	distance along the surface measured from the stagnation point
V	velocity
$X(y)$	shock-wave shape (origin on shock)
x,y	cylindrical coordinates with origin at stagnation point on body
γ	isentropic exponent
Δ	shock standoff distance
θ	stream angle
θ_c	cone angle
ρ	density

Subscripts

o	free-stream conditions at stagnation point location
st	stagnation point
unif	uniform flow
∞	free-stream conditions just upstream of bow wave

METHOD OF SOLUTION

The flow field around a body of revolution immersed in a spherical source flow satisfies the condition of axial symmetry (see fig. 1). Therefore, the computer programs described in reference 5 are applicable, provided the

variations in free-stream conditions upstream of the bow wave are properly taken into account. The corresponding two-dimensional problem, a plane-symmetric body in a cylindrical source flow, can also be treated but is not considered here. The programs can be described briefly as follows: an inverse method is used for the subsonic-transonic region; that is, a shock shape is assumed, and the corresponding body shape is calculated. Iteration of the shock shape is usually necessary to obtain the desired body shape. The method of characteristics is then used to continue the solution in the supersonic region.

The equations of motion have the same form as those presented in reference 5. The source flow appears only through the boundary conditions upstream of the bow wave. A source flow parameter is defined as R_b/L_o where R_b is the radius of curvature of the body at the stagnation point, and L_o is the distance between the source and the stagnation point on the body (see fig. 1). Note that the size of the body relative to the nozzle length is the significant parameter and not the nozzle angle. The free-stream conditions at the apex of the shock wave ($x = -\Delta$) are assumed known and those downstream are calculated for classical source flow (see ref. 6). The free-stream conditions other than the stream angle depend solely on the distance, L; the stream angle is determined simply from geometrical considerations.

The method of reference 5 is limited essentially by the ability to find a solution for the subsonic-transonic region. It was found in reference 7 that a shock shape described by a one-parameter rational polynomial would yield spheres and not too blunt ellipsoids. This shock shape has been altered slightly to provide even symmetry about the axis and can be written as

$$\left(\frac{X_{unif}}{R_s}\right)^2 = \frac{\frac{1}{4}\left(\frac{y}{R_s}\right)^4 + A_7\left(\frac{y}{R_s}\right)^6}{1 + \frac{4A_7}{M_o^2 - 1}\left(\frac{y}{R_s}\right)^4} \tag{1}$$

where R_s is the radius of curvature of the shock at the axis, and A_7 is the parameter nearly equal to A_5 which is plotted in reference 7 for a wide range of free-stream conditions.

The principal effect of the source flow in the nose region is the finite stream angle away from the axis. One would expect the shock-wave angle or slope to change locally in the same manner. After trying various shock shapes, we found that spheres in a source flow can be obtained by perturbation of the slope of the shock shape given by equation (1) as follows:

$$\frac{dX}{dy} = \left[1 - C_1\sqrt{\left(\frac{y}{R_s}\right)^2 + C_2\left(\frac{y}{R_s}\right)^{C_3}}\right]\frac{dX_{unif}}{dy} \tag{2}$$

The equation for the shock shape cannot be written explicitly, but the coordinates can be determined readily by numerical integration. With $C_3 < 1$, the bracketed term in equation (2) behaves as $1 - C_1(y/R_s)$ for large values of y and as $1 - C_1\sqrt{C_2(y/R_s)^{C_3}}$ for small values of y. The latter term was found necessary to obtain a smooth body shape in the stagnation region. For perfect gas solutions it has been found that C_1 is a function of both R_b/L_o and γ, C_2 is just a function of γ, and $C_3 = 0.125$, a constant.

The procedure used to obtain the blunt-body solutions described in the present report can be outlined as follows:

1. The value of the shock-wave parameter, A_7, is found for a uniform flow.

2. A value of C_2 is selected, depending on γ.

3. For the given value of R_b/L_o, the value of C_1 is optimized to obtain the best fit to the desired body shape.

Neither the procedure nor the shock shape employed in this study is to be considered unique; however, they have been successful in obtaining satisfactory solutions over a wide range of free-stream conditions. For extreme source flow problems, it may be advantageous to modify this procedure somwhat although in these instances numerical difficulties described in reference 7 may preclude any satisfactory solution. As in the uniform flow case, the numerical difficulties arise with decreasing Mach number and increasing values of body bluntness and γ.

The flow field in the supersonic region is calculated by the method of characteristics beginning with data along a noncharacteristic line obtained from the blunt-body solution. The body shape is an arbitrary input, and the shock shape is computed. The sole change made in the program described in reference 5 is the allowance for nonuniform conditions upstream of the bow wave.

RESULTS AND DISCUSSION

Perfect gas solutions have been obtained for the following range of free-stream conditions

$$\gamma = 1.2,\ 1.4,\ 1.6667$$

$$M_o = 10,\ 20,\ 40$$

$$0 \leq \frac{R_b}{L_o} \leq 0.08$$

in order to demonstrate the quantitative effect of source flow on shock-wave shape, standoff distance, stagnation-point velocity gradient, and surface-pressure distribution. These results should indicate qualitatively the effect of source flow for other free-stream conditions including dissociated and ionized streams and also serve as a guide in using the present calculation method to obtain solutions for specific cases of flow conditions and model geometry. The flow in the subsonic-transonic region of spherical and ellipsoidal noses calculated by the inverse method will be considered initially. Then the flow in the supersonic region around hemisphere-cylinders and spherically blunted cones calculated by the method of characteristics will be studied. Comparisons will be made with predictions of approximate methods, wherever possible, in order to evaluate their usefulness.

Spherical Nose

A résumé of solutions for a spherical nose is presented in table I. Values of the shock parameter, C_1, required in equation (2), are shown in figure 2 for $M_0 = 20$ as a function of the source flow parameter, R_b/L_0. The dependence on Mach number is negligible so that these values apply for $10 \leq M_0 \leq 40$. Values of C_2 are presented in table I, and a value of 0.125 was used for C_3. Because of numerical difficulties described in reference 7, satisfactory solutions were not obtained for the complete range of free-stream conditions (for the larger values of γ and smaller values of Mach number), at least by using the procedure outlined previously in the Method of Solution section.

The effect of the source flow is to decrease the standoff distance and radius of curvature of the shock at the axis so that it lies inside the uniform flow shock in the stagnation region and outside the uniform flow shock over the afterbody. A typical comparison of shock shapes is shown in figure 3 for $\gamma = 1.4$ and $M_0 = 20$. (The portion of the shock for $y/R_b \gtrsim 0.8$ was calculated by the method of characteristics.) The ratio of the nose radius to the shock radius, the shock standoff distance, and the stagnation-point velocity gradient are shown in figure 4 for $M_0 = 20$. The dependence of these quantities on the source flow parameter is nearly linear. The shock standoff distance decreases as noted previously; whereas, the ratio of the nose radius to the shock radius and the stagnation-point velocity gradient increase with source flow. Normalized by their respective uniform flow values as in figure 4, the dependence of these quantities on Mach number for $10 \leq M_0 \leq 40$ is nearly eliminated and the dependence on γ is minimized. The results for $\gamma = 1.2$ and 1.4 are nearly the same, but the results for $\gamma = 1.6667$ are affected more by source flow.

Shown for comparison in figure 4 are the predictions of Berndt (ref. 1), who used the constant-density approximation to study analytically the effect of source flow in the stagnation region. Berndt's theory underestimates the effect of source flow on the shock standoff distance and stagnation-point velocity gradient. In addition, Berndt's theory predicts that these quantities normalized by their uniform flow values are essentially independent of γ, whereas, the present method shows some dependence on γ.

Consistent with the increase in the stagnation-point velocity gradient shown in figure 4(c) is the decrease in the surface pressure away from the stagnation point with source flow as shown in figure 5 for $\gamma = 1.4$ and $M_o = 20$. The pressure distributions for $\gamma = 1.2$ and 1.6667 and $M_o = 10$ and 40 are practically identical with the distributions shown in figure 5. Shown for comparison are the predictions of modified Newtonian theory which includes both the effect of finite stream angle and varying free-stream properties but does not include any centrifugal corrections. Although modified Newtonian theory predicts higher surface pressures than the present method, the theory does predict quite satisfactorily the reduction in surface pressure with source flow.

The pressure distributions over the hemisphere have been integrated to obtain the drag coefficient shown in figure 6. (The flow in the supersonic region for the present method was calculated by the method of characteristics.) The reduction in drag coefficient with source flow is nearly linear and of the same order of magnitude as R_b/L_o. Modified Newtonian theory predicts higher drag coefficients than the present method, but it does predict satisfactorily the reduction in drag coefficient with source flow.

Ellipsoidal Nose

A résumé of solutions for an ellipsoidal nose with bluntness, $B_b = 2.25$, is presented in table II for $M_o = 20$ and $\gamma = 1.2$ and 1.4. The method of solution was essentially the same as the one used for a spherical nose. First, the value of A_7 in equation (1) was found for an ellipsoidal nose in a uniform stream; then the optimum value of C_1 in equation (2) was found with source flow. The values of C_1 are shown in figure 7 as a function of the source flow parameter R_b/L_o, where R_b is the radius of curvature of the ellipsoid at the stagnation point. The use of R_b as the reference length results in C_1 having nearly the same values as shown in figure 2 for a spherical nose. Since the program does not work as well for blunt ellipsoids as it does for spheres, more scatter is evident in the present results.

The ratio of nose radius to shock radius, the shock standoff distance, and the stagnation-point velocity gradient for the ellipsoidal nose are shown in figure 8, with all the quantities normalized by their respective uniform flow values. With R_b/L_o as the source flow parameter, the results are similar to those for a spherical nose shown in figure 4. The dependence on γ is not clearly defined; at least, the differences in the results for $\gamma = 1.2$ and 1.4 as normalized in figure 8 are not appreciable.

The preceding solutions for the subsonic-transonic region have shown that the effect of source flow on the ratio of nose radius to shock radius, shock standoff distance, stagnation-point velocity gradient, and surface pressure distribution is proportional to the source flow parameter, R_b/L_o. In addition, the changes in these quantities are of the same order of magnitude as the value of R_b/L_o.

Hemisphere Cylinder

The flow in the supersonic region of a hemisphere cylinder has been calculated by the method of characteristics for $\gamma = 1.4$ and $M_o = 20$ to demonstrate the effects of source flow for values of R_b/L_o up to 0.06. The shock wave is displaced outward as shown in figure 9. Before considering the surface pressure distributions, it is of interest to examine the effect of source flow on the local free-stream properties just upstream of the shock wave. Marked reductions of pressure and density occur as shown in figure 10. The Mach number increases slightly, but the velocity, which is not shown, changes negligibly. For small values of the source flow parameter, essentially the same conditions prevail along the nozzle axis. On the basis of isentropic flow relationships, the changes in free-stream conditions would be larger for larger values of γ.

The surface-pressure distributions normalized by the stagnation-point pressure and the reductions in surface pressure normalized by the local uniform flow value are shown in figures 11(a) and 11(b), respectively. The effect of source flow is to cause significant reductions in surface pressure that are an order of magnitude greater than the value of the source flow parameter. The fluctuations on the hemisphere (see fig. 11(b)) are partially due to small errors resulting from defining the body shape with polynomials passing through a discrete set of coordinates. This method of specifying the body shape was necessary in order to join the method of characteristics solution smoothly to the inverse solution for the subsonic-transonic region. Otherwise, errors in the body slope of a few percent in the inverse solution at the matching point would have caused an imbedded shock in the flow field.

The reductions in surface pressure shown in figure 11(b) display two distinct regions. Over the hemisphere the reduction in surface pressure increases sharply with axial distance; over the cylindrical afterbody the variation is not so steep. The effect is greater for increasing values of γ. An examination of figures 10 and 11 shows that the reduction in surface pressure with source flow at a given body station is of the same order of magnitude as the reduction in free-stream pressure at the same axial location. This occurs even though the portion of the free stream that influences a particular body station is located much closer to the nose. To illustrate this point, a right-running characteristic is sketched in figure 9 for $R_b/L_o = 0$ to indicate the portion of the shock wave that influences the flow over the afterbody for $x/R_b < 10$.

In reference 2, Hall presents a theory that assumes the effect of source flow on shock-wave shape and surface-pressure distribution can be expressed as small perturbations of the uniform flow values. This theory predicts quite well the displacement of the shock wave as shown in figure 9, but fails to predict quantitatively the surface pressures except for isolated regions as shown in figure 11(a). In figure 11(b) Hall's theory is shown to predict a reduction in surface pressure that varies linearly with axial distance from the nose. The magnitude of the reduction is directly proportional to the source flow parameter, R_b/L_o, and is larger for increasing values of γ (not shown). It is apparent that the surface pressure would eventually vanish according to this theory, for instance, at $x/R_b = 10$ for $R_b/L_o = 0.06$. However, these

reductions in pressure are not small perturbations so the theory would not be expected to be valid under these circumstances. In general, Hall's theory predicts only qualitatively the effect of source flow on surface pressure distribution.

Calculations have been performed for an ellipsoid cylinder with $B_b = 2.25$, $\gamma = 1.4$, and $M_o = 20$ and for $b/L_o = 0, 0.02, 0.04$. Although the surface-pressure distributions along the cylindrical afterbody for uniform flow were somewhat different from the spherical nose solutions, the reductions in surface pressure with source flow were within a few percent of the curves shown in figure 11(b). The effect of the nose shape is apparently negligible if the reduction in surface pressure is normalized by the uniform flow value.

The fact that the effect of the nose shape or solution on the afterbody flow appears negligible suggests an approximate technique. Eaves and Lewis in reference 4 performed calculations for blunt-nosed bodies in source flow with the assumption that the flow in the subsonic-transonic region was identical to that for a uniform flow. It has been shown previously that this assumption is not correct, that differences of the same order of magnitude as the source flow parameter do occur. However, the effect on the afterbody flow may be negligible. Calculations have been performed to test the validity of this assumption. In figure 12, there is shown the pressure distribution on a hemisphere cylinder for $\gamma = 1.4$, $M_o = 18$, and $R_b/L_o = 0.0219$. The abscissa in this figure is the distance along the surface normalized by R_b. The results from reference 4 and the present method agree within acceptable limits.

The present method was also modified to solve the source flow problem with input points provided by a uniform flow blunt-body solution, similarly to the method of reference 4. These results are also in agreement. A close examination of the flow field showed that an expansion wave propagates from the initial shock point to the body surface, quickly adjusting the pressure to nearly the correct value with source flow. A comparison of exact and approximate solutions for $R_b/L_o = 0.06$ in figure 12 again shows reasonable agreement. One can conclude that as far as the pressure distribution over the afterbody is concerned, the use of a uniform flow blunt-body solution for the subsonic-transonic region provides satisfactory results.

Spherically Blunted Cones

The flow fields around spherically blunted 15° and 30° cones have been calculated for $\gamma = 1.4$ and $M_o = 20$ to demonstrate the effects of source flow for values of R_b/L_o up to 0.06. The shock-wave configurations are shown in figure 13. The outward displacement of the shock wave for the 15° cone with source flow is similar to that shown for a hemisphere cylinder in figure 9. On the other hand, the shock wave for the 30° cone is not affected appreciably by the source flow. This difference in behavior can be described as follows: For blunted slender cones, including the hemisphere cylinder as a limiting case, the shock-wave shape is determined essentially by the forebody shape, which is a hemisphere, and is displaced outward with source flow. For blunted cones with large vertex angles including the 30° cone, the shock wave conforms to the afterbody shape and is influenced only slightly by the source flow.

Consequently, caution should be exercised in evaluating source flow effects on blunted cones from shock-shape measurements.

The surface-pressure distributions normalized by the stagnation-point pressure are shown in figure 14, and the reductions in surface pressure normalized by the uniform flow value are shown in figure 15. The predictions of modified Newtonian theory are shown for comparison. With source flow, the pressure on the conical surface does not asymptotically approach the sharp cone value after the over expansion behind the nose, but instead eventually decays to zero. Comparison of figures 11(b) and 15 shows that in the vicinity of the nose, the reduction in surface pressure is of the same order of magnitude for both a hemisphere cylinder and blunted cones. Downstream from the nose, the reductions in pressure are greater for the blunted cones. In this region of the 30° cone, modified Newtonian theory predicts quite well the reduction in surface pressure with source flow as shown in figure 15. This result is consistent with the relative insensitivity to source flow of the shock shape, which in the Newtonian approximation is assumed to conform to the body shape.

COMPARISONS WITH EXPERIMENTAL RESULTS

Both the Ames arc-heated plasma facility and the 1-foot shock tunnel utilize conical nozzles. Data obtained in these facilities will now be compared with the predictions of the present numerical method. Lacking knowledge of the actual distribution of free-stream conditions in the nozzles, ideal spherical source flow will be assumed. The distance from the source to the model, L_o, is calculated from the nozzle geometry without any boundary-layer corrections. The free-stream conditions are assumed known at the stagnation point of the model (essentially the same conditions prevail at the apex of the bow shock), and the free-stream conditions downstream are readily calculable. No boundary-layer corrections are made for the model. The predictions from the present method thus represent the maximum probable effect of source flow.

Hemisphere Tested in Arc Tunnel

The Ames arc-heated plasma facility produces stagnation enthalpies ranging from 10 to 20 MJ/kg with nitrogen as the test gas. For the tests conducted by Mr. Lewis Anderson and reported here, the value of the ideal source flow parameter, R_b/L_o, was 0.084 (see fig. 16). The stream was believed to be frozen with $\gamma \approx 1.46$ and $M_o \approx 7.3$ according to pressure measurements. Perfect gas flow with $\gamma = 1.4$ and $M_o = 8$ was assumed in the present method. It has been shown previously that the effect of γ on the surface pressure distribution in the subsonic region is negligible. Since the free-stream conditions were outside the range covered in table I, the method used to optimize the shock shape parameters was modified slightly. The value of A_7 in equation (1) was optimized to be 0.047 after setting in equation (2), $C_1 = 0.036$, $C_2 = 10.0$, and $C_3 = 0.0625$.

Unpublished surface pressure data for a hemisphere normalized by the stagnation-point pressure is shown in figure 16. The present method predicts

the surface pressure for $s/R_b < 1$, but the data for $s/R_b > 1$ appears to have some extraneous afterbody or tunnel effect. The stagnation-point velocity gradient was calculated from the measured surface pressures by Mr. Lewis Anderson with the assumption of isentropic flow away from the stagnation point. The gradient was found to be 20 percent larger than the value determined in a tunnel with a uniform stream. This increase was consistent with the higher measured stagnation-point heat-transfer rates. However, the present numerical method predicts only a 10-percent increase in the stagnation-point velocity gradient with source flow.

Hemisphere Cylinder Tested in Shock Tunnel

The Ames 1-foot shock tunnel has been operated with various test gases at a stagnation enthalpy of 8 MJ/kg. Pressure and heat-transfer measurements have been reported by Marvin and Akin in reference 8, from which the following results are taken. The value of the ideal source flow parameter was equal to 0.0278. With argon as the test gas, the flow was believed to be in equilibrium. The procedure followed to obtain a solution for a real gas is the same as for a perfect gas. For the shock-tunnel conditions listed in figure 17, the values of the shock parameters for a spherical nose were $A_7 = 0.0355$, $C_1 = 0.01345$, $C_2 = 10.0$, and $C_3 = 0.125$.

The surface pressure measurements on a hemisphere cylinder reported in reference 8 are reproduced in figure 17. The test data lie below the predictions from the present method for a uniform flow. The predicted reduction of surface pressure with source flow is significant; for $s/R_b = 7$, the reduction is 40 percent. The experimental results now lie properly above the predictions, part of the difference being attributable to viscous effects on both the nozzle and the model. There still remains the uncertainty in the chemistry of the flow.

CONCLUDING REMARKS

The effect of spherical source flow about blunt-nosed axisymmetric bodies has been studied by modifying existing computer programs to account for the nonuniform free stream. Solutions have been obtained for spherical noses in perfect gas flow for values of the source flow parameter up to 0.08, where the parameter is defined as the ratio of the nose radius of curvature to the distance between the source and the nose. These results demonstrate the following qualitative effects of source flow. In the subsonic-transonic region, the stagnation-point velocity gradient increases and the shock standoff distance and surface pressure decrease with source flow, the relative changes being of the same order of magnitude as the source flow parameter. In the supersonic region over cylindrical and conical afterbodies, the surface pressure decreases, with the percentage reduction being an order of magnitude greater than the source flow parameter. The shock wave is displaced outward, but this effect is small for a spherically blunted 30° cone.

Comparisons with predictions of approximate theories and methods showed the following results: For the nose region, a constant-density solution underestimated the effects of source flow on standoff distance and stagnation-point velocity gradient. For the afterbody region, an analysis based on small perturbations of the uniform flow solution failed to predict quantitatively the surface-pressure distribution, but it did predict the displacement of the shock wave. Modified Newtonian theory was shown to predict quite closely the reduction in surface pressure with source flow in the subsonic region of a spherical nose and over the conical portion of a blunted 30° cone. Since the nose solution does not affect greatly the flow over the afterbody, an approximate method that joins a method of characteristics solution including source flow with a blunt-body solution for a uniform flow was found to yield satisfactory results. Comparisons have also been made with experimental results from models tested in conical nozzles; these results indicate that source flow effects can be predicted satisfactorily.

In conclusion, source flow effects have been found to be significant, especially on afterbody pressure distributions. Caution should be exercised in using approximate theories to predict source flow effects. The present calculation method can be used to solve numerically the exact equations of motion over a wide range of free-stream conditions. The examples presented in this report should serve as a guide in obtaining solutions for a particular set of free-stream conditions and model geometry.

Ames Research Center
National Aeronautics and Space Administration
Moffett Field, Calif., Jan. 17, 1966

REFERENCES

1. Berndt, Sune B.: On the Influence of the Non-Uniform Free-Stream of a Conical Wind Tunnel Nozzle on the Axisymmetric Hypersonic Flow Around Blunt Bodies. Aeronaut. Rep. LR-338, Nat. Aeronaut. Estab. (Canada), Feb. 1962.

2. Hall, J. Gordon: Effects of Ambient Nonuniformities in Flow Over Hypersonic Test Bodies. Cornell Aeronaut. Lab. Rep. 128, Aug. 1963.

3. Baradell, Donald L.; and Bertram, Mitchel H.: The Blunt Plate in Hypersonic Flow. NASA TN D-408, 1960.

4. Eaves, R. H. Jr.; and Lewis, Clark H.: Combined Effects of Viscous Interaction and Ideal Source Flow on Pressure and Heat-Transfer Distributions Over Hemisphere Cylinders at $M_\infty \sim 18$. AEDC-TR-65-158, ARO, Inc., Arnold Air Force Station, Tenn., July 1965.

5. Inouye, Mamoru; Rakich, John V.; and Lomax, Harvard: A Description of Numerical Methods and Computer Programs for Two-Dimensional and Axisymmetric Supersonic Flow Over Blunt-Nosed and Flared Bodies. NASA TN D-2970, 1965.

6. Sauer, Robert: Introduction to Theoretical Gas Dynamics. Translated by Freeman K. Hill and Ralph A. Alpher, J. W. Edwards, Ann Arbor, 1947.

7. Lomax, Harvard; and Inouye, Mamoru: Numerical Analysis of Flow Properties About Blunt Bodies Moving at Supersonic Speeds in an Equilibrium Gas. NASA TR R-204, 1964.

8. Marvin, Joseph G.; and Akin, Clifford M.: Pressure and Convective Heat Transfer Measurements in a Shock Tunnel Using Several Test Gases. NASA TN D-3017, 1965.

TABLE I.- RÉSUMÉ OF SOLUTIONS FOR SPHERES

γ	C_2	M_o	A_7	$\frac{R_b}{L_o}$	C_1	$\frac{R_b}{R_s}$	$\frac{\Delta}{R_s}$	$\frac{\Delta}{R_b}$	$\frac{R_b}{V_o}\left(\frac{dV}{ds}\right)_{st}$
1.2	5.0	10	0.0956	0	0	0.840	0.0655	0.0779	0.473
				.01	.00705	.850	.0654	.0770	.480
				.02	.01353	.859	.0653	.0760	.486
				.03	.01958	.868	.0652	.0751	.493
				.04	.02437	.875	.0650	.0743	.497
				.05	.03043	.885	.0649	.0734	.505
				.06	.03606	.894	.0648	.0726	.511
				.07	.04141	.902	.0647	.0717	.518
		20	.1006	0	0	.853	.0619	.0725	.460
				.01	.00720	.863	.0618	.0716	.466
				.02	.01355	.872	.0617	.0708	.473
				.03	.01974	.882	.0616	.0699	.478
				.04	.02546	.890	.0615	.0691	.484
				.05	.03096	.899	.0614	.0683	.490
				.06	.03658	.908	.0613	.0676	.498
				.07	.04185	.917	.0612	.0668	.505
				.08	.04684	.925	.0611	.0660	.513
		40	.1018	0	0	.856	.0610	.0712	.455
				.01	.00729	.867	.0609	.0703	.462
				.02	.01360	.876	.0608	.0694	.469
				.03	.01977	.885	.0607	.0686	.475
				.04	.02560	.894	.0606	.0678	.481
				.05	.03111	.902	.0605	.0671	.486
				.06	.03665	.912	.0604	.0663	.495
				.07	.04178	.920	.0603	.0656	.501
				.08	.04678	.929	.0602	.0648	.509
1.4	10.0	10	.0780	0	0	.761	.1032	.1356	.599
				.01	.00502	.770	.1030	.1337	.607
				.02	.01005	.780	.1028	.1318	.616
				.03	.01452	.789	.1027	.1302	.622
				.04	.01938	.798	.1025	.1283	.631
				.05	.02360	.808	.1024	.1267	.637
				.06	.02896	.819	.1021	.1246	.649
		20	.0815	0	0.	.771	.1004	.1302	.592
				.01	.00498	.780	.1002	.1284	.600
				.02	.00982	.790	.1000	.1267	.609
				.03	.01434	.799	.0999	.1250	.616
				.04	.01892	.808	.0997	.1234	.621
				.05	.02325	.818	.0996	.1218	.628
				.06	.02744	.827	.0994	.1202	.636
		40	.0827	0	0	.774	.0997	.1289	.590
				.01	.00500	.783	.0995	.1271	.599
				.02	.01000	.792	.0993	.1253	.608
				.03	.01432	.801	.0992	.1238	.612
				.04	.01891	.811	.0990	.1221	.620
				.05	.02321	.820	.0988	.1205	.627
				.06	.02737	.829	.0987	.1190	.635
1.6667	40.0	10	.0665	0	0	.687	.1401	.2039	.700
				.01	.00307	.698	.1400	.2004	.713
		20	.0692	0	0	.696	.1380	.1983	.693
				.01	.00301	.707	.1379	.1951	.707
				.02	.00596	.718	.1377	.1918	.719
				.03	.00881	.729	.1375	.1886	.736
		40	.0700	0	0	.698	.1374	.1970	.693
				.01	.00301	.709	.1373	.1937	.706
				.02	.00594	.720	.1372	.1905	.718
				.03	.00877	.731	.1370	.1874	.732

TABLE II.- RÉSUMÉ OF SOLUTIONS FOR ELLIPSOIDS, $B_b = 2.25$

γ	C_2	M_o	A_7	$\frac{R_b}{L_o}$	C_1	$\frac{R_b}{R_s}$	$\frac{\Delta}{R_s}$	$\frac{\Delta}{R_b}$	$\frac{R_b}{V_o}\left(\frac{dV}{ds}\right)_{st}$
1.2	5.0	20	0.2628	0.	0	0.904	0.0622	0.0688	0.478
				.015	.01176	.918	.0622	.0677	.487
				.030	.02092	.930	.0620	.0667	.496
				.045	.03332	.947	.0621	.0656	.509
				.060	.04650	.966	.0623	.0644	.523
				.075	.05711	.982	.0623	.0634	.535
1.4	10.0	20	.1998	0	0	.846	.1013	.1197	.419
				.015	.00747	.858	.1009	.1176	.432
				.030	.01406	.869	.1006	.1158	.440
				.045	.02040	.881	.1003	.1139	.446
				.060	.02687	.893	.1002	.1122	.456

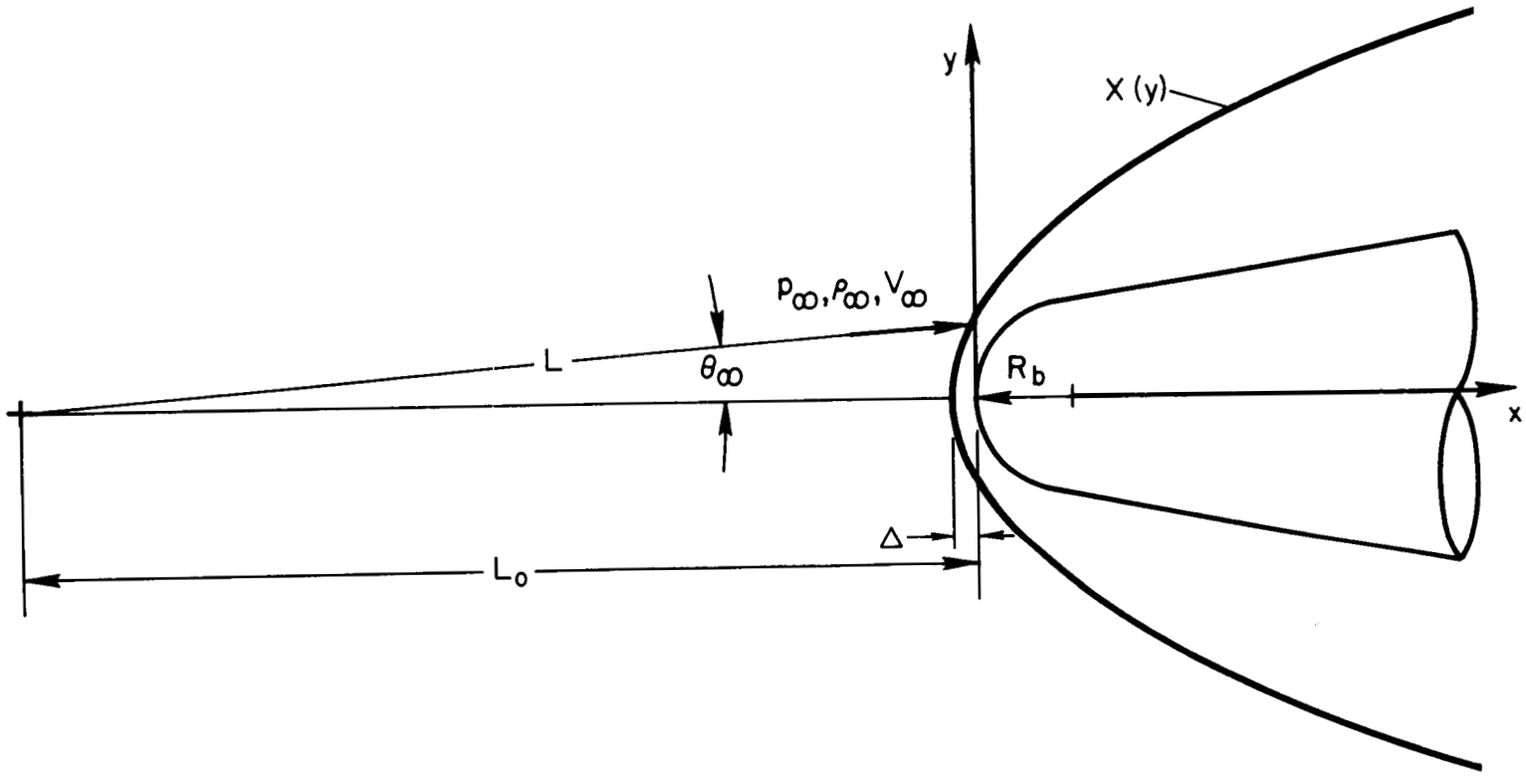

Figure 1.- Coordinate system.

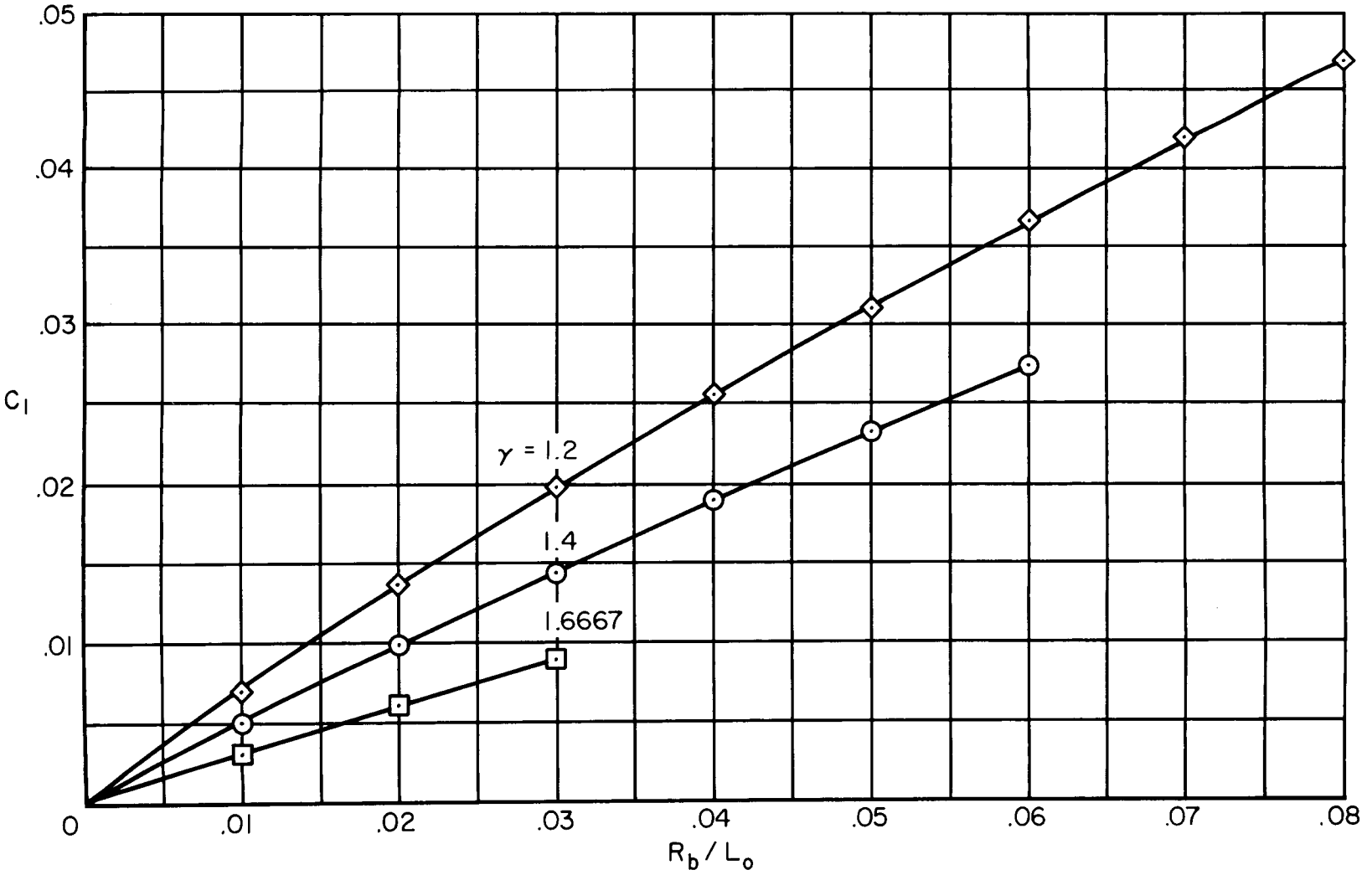

Figure 2.- Shock shape parameter, C_1, for spherical nose in source flow; M_o = 20.

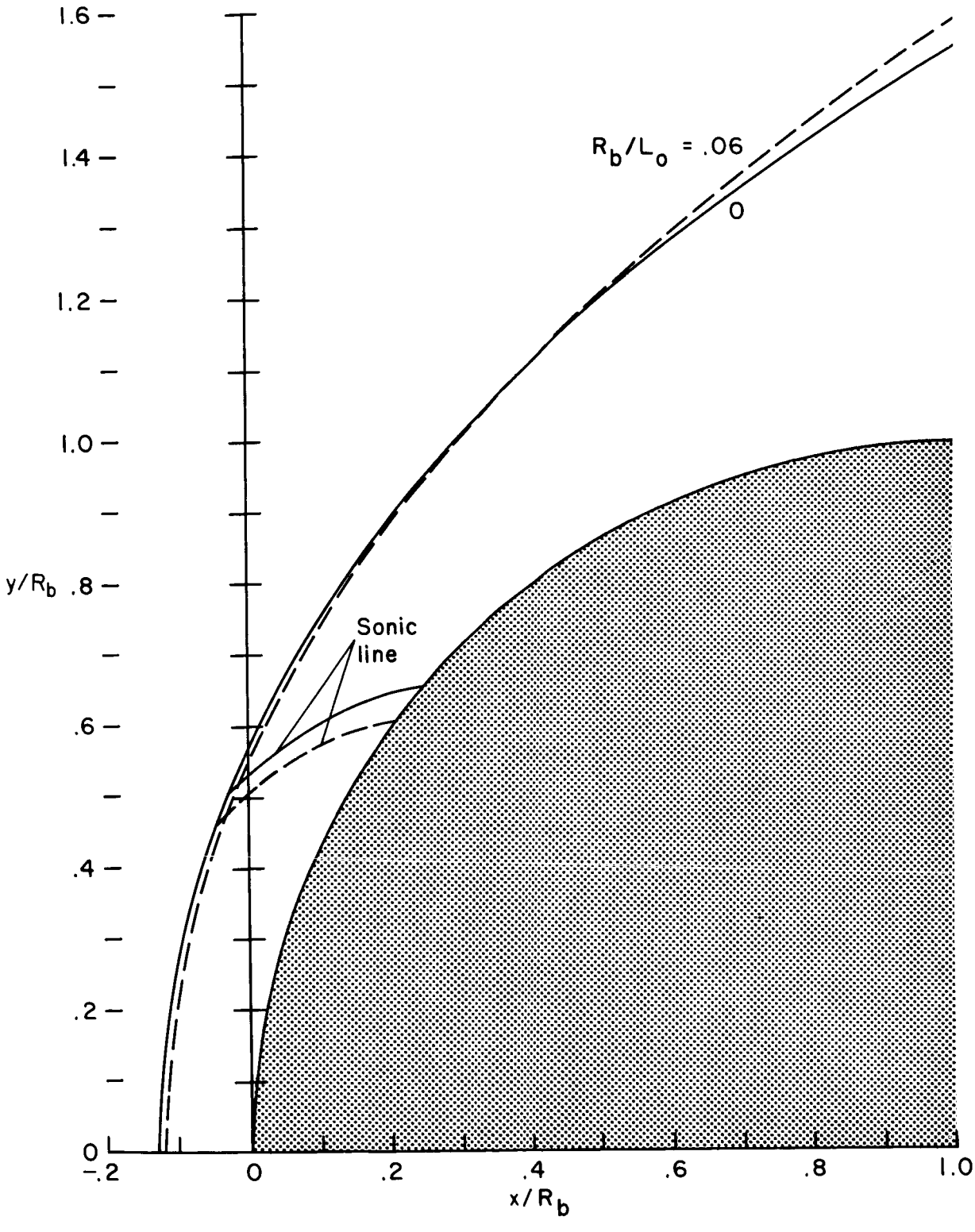

Figure 3.- Shock-wave shape for spherical nose; $\gamma = 1.4$, $M_o = 20$.

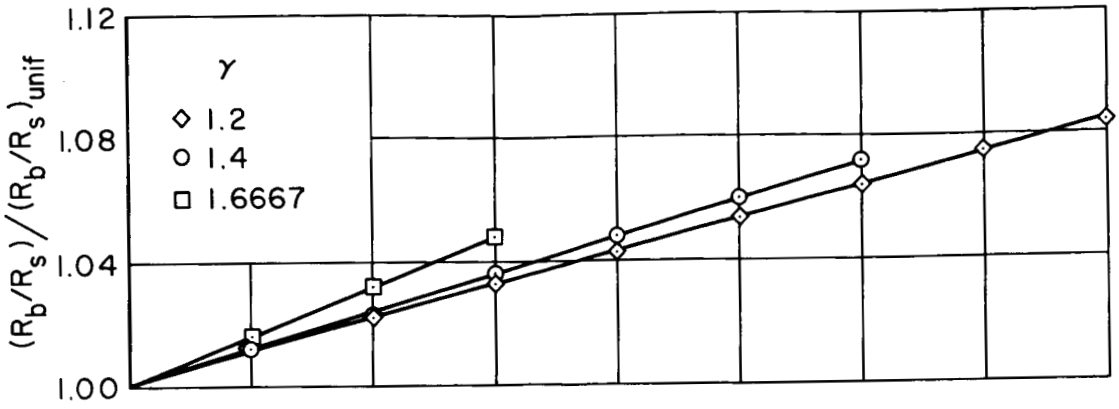

(a) Ratio of nose radius to shock radius.

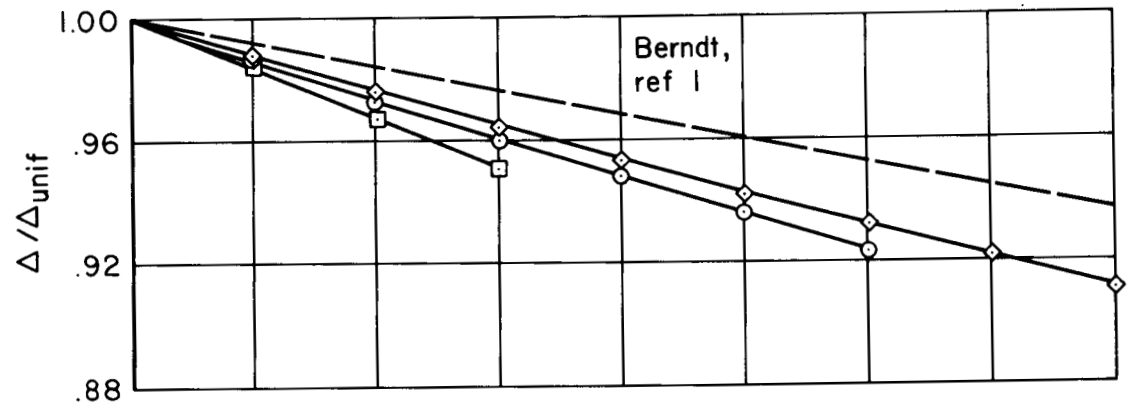

(b) Shock standoff distance.

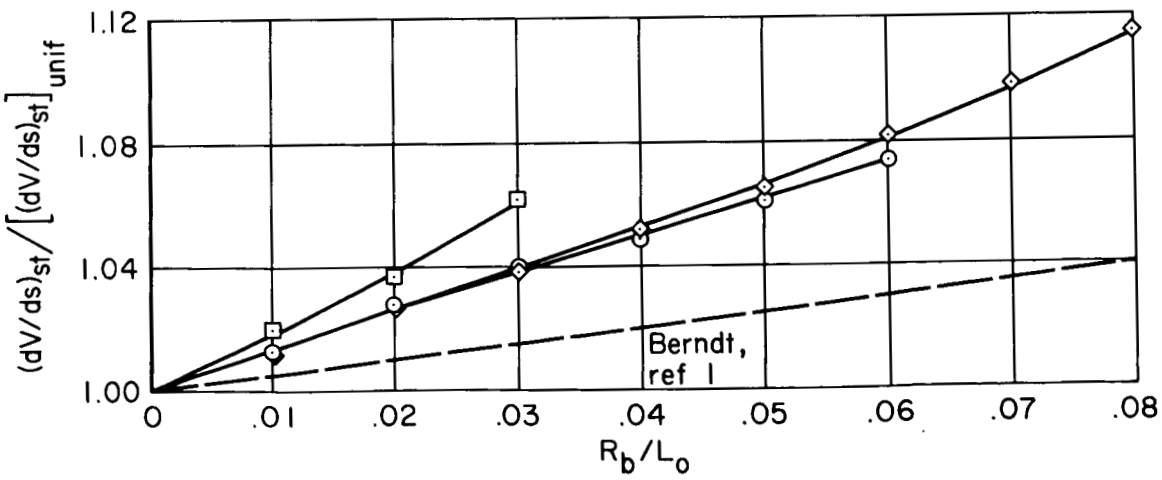

(c) Stagnation-point velocity gradient.

Figure 4.- Ratio of nose radius to shock radius, shock standoff distance, and stagnation-point velocity gradient normalized by uniform flow values for spherical nose; $M_\infty = 20$.

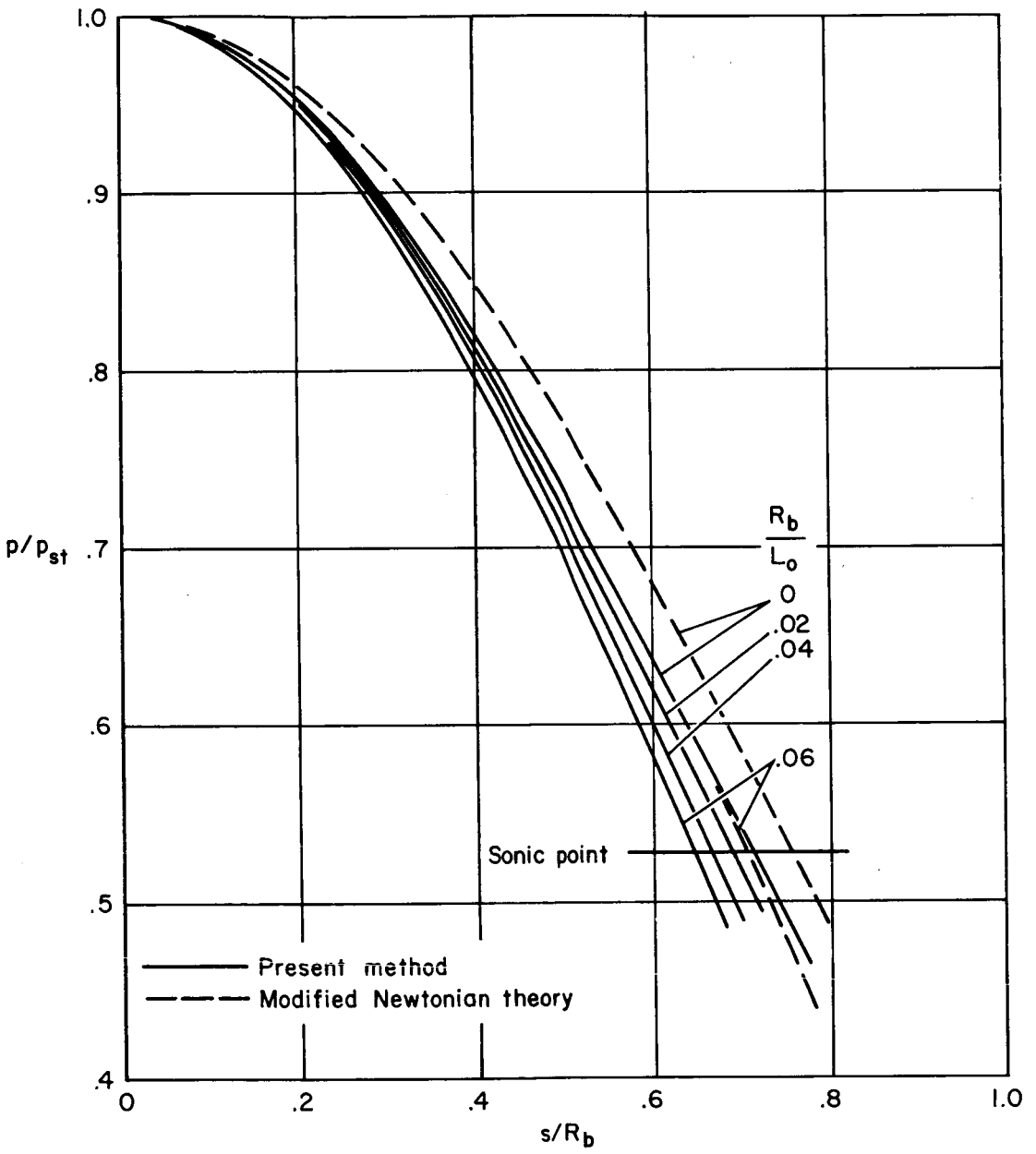

Figure 5.- Surface-pressure distribution for spherical nose; $\gamma = 1.4$, $M_o = 20$.

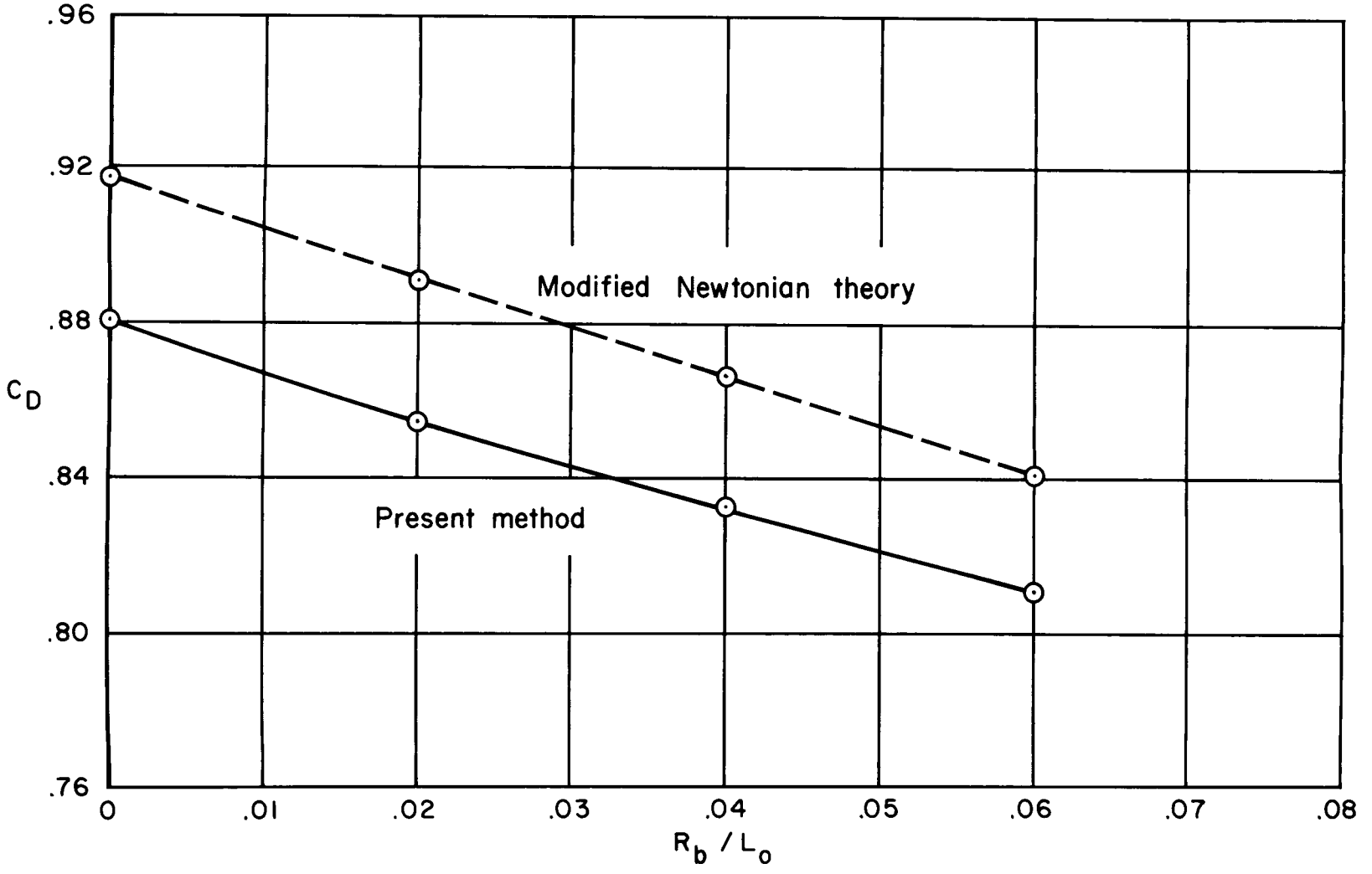

Figure 6.- Drag coefficient for hemisphere; $\gamma = 1.4$, $M_\infty = 20$.

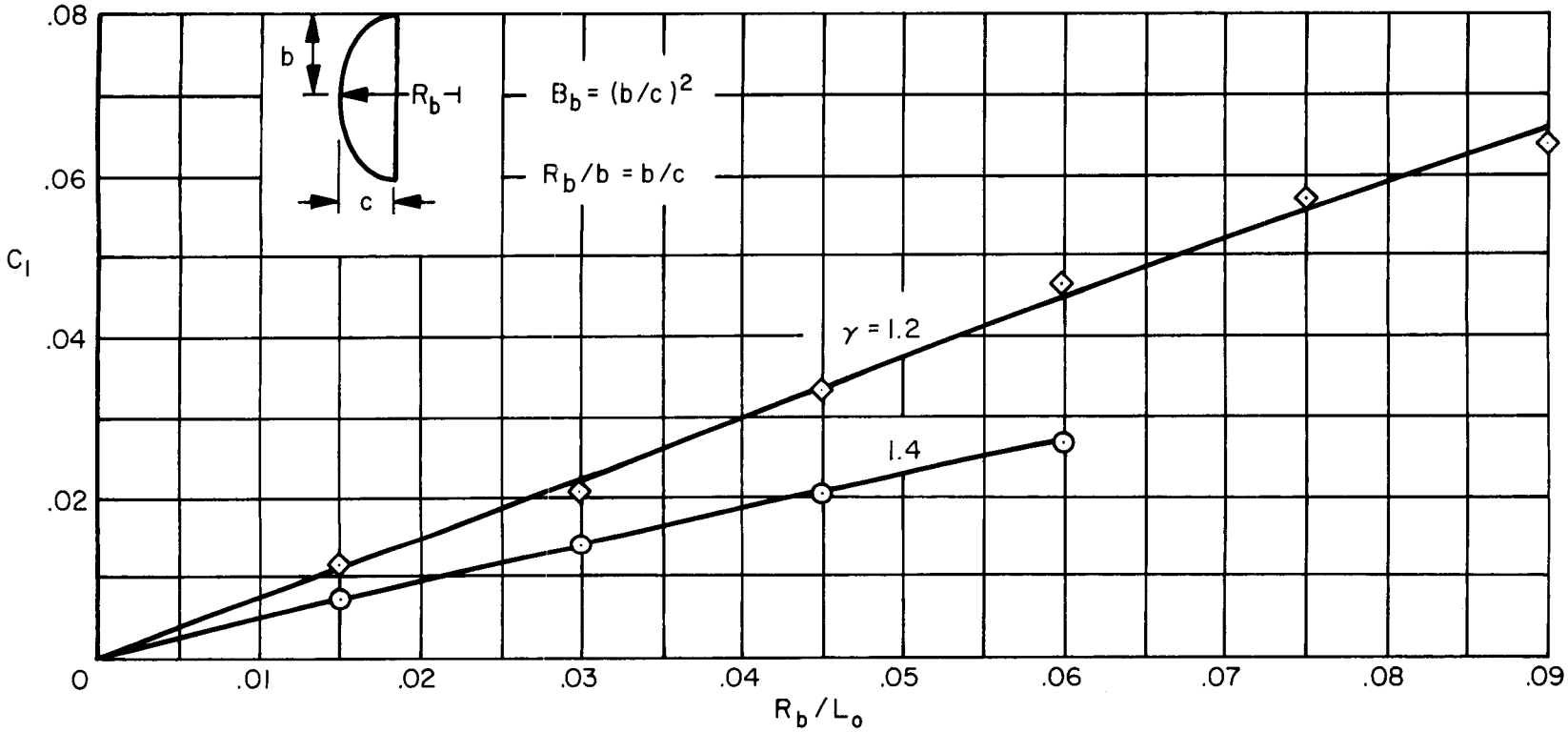

Figure 7.- Shock shape parameter, C_1, for ellipsoidal nose in source flow; $B_b = 2.25$, $M_o = 20$.

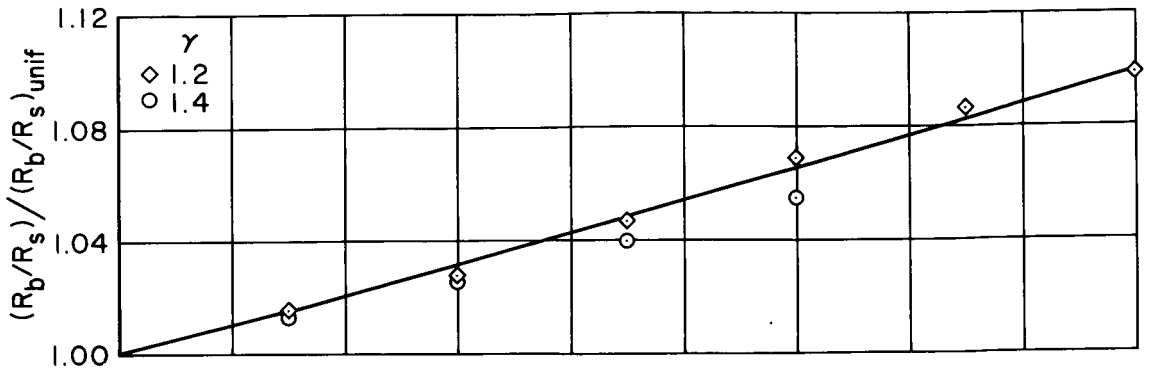

(a) Ratio of nose radius to shock radius.

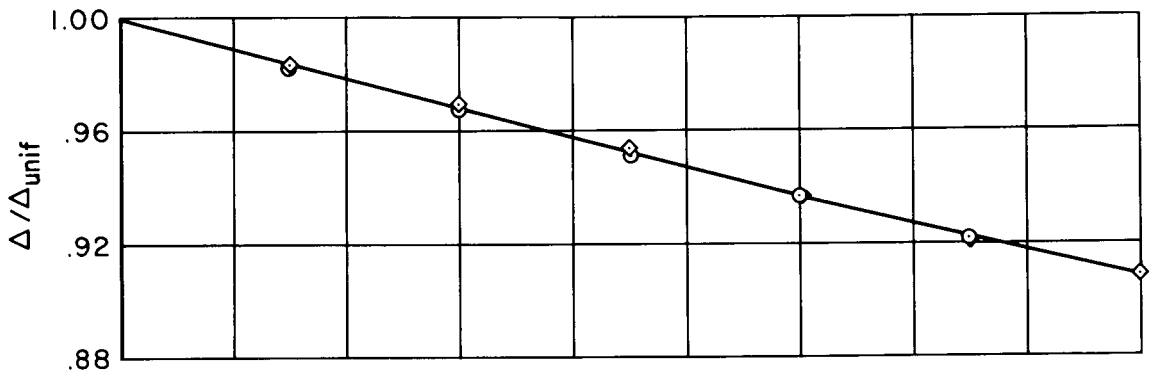

(b) Shock standoff distance.

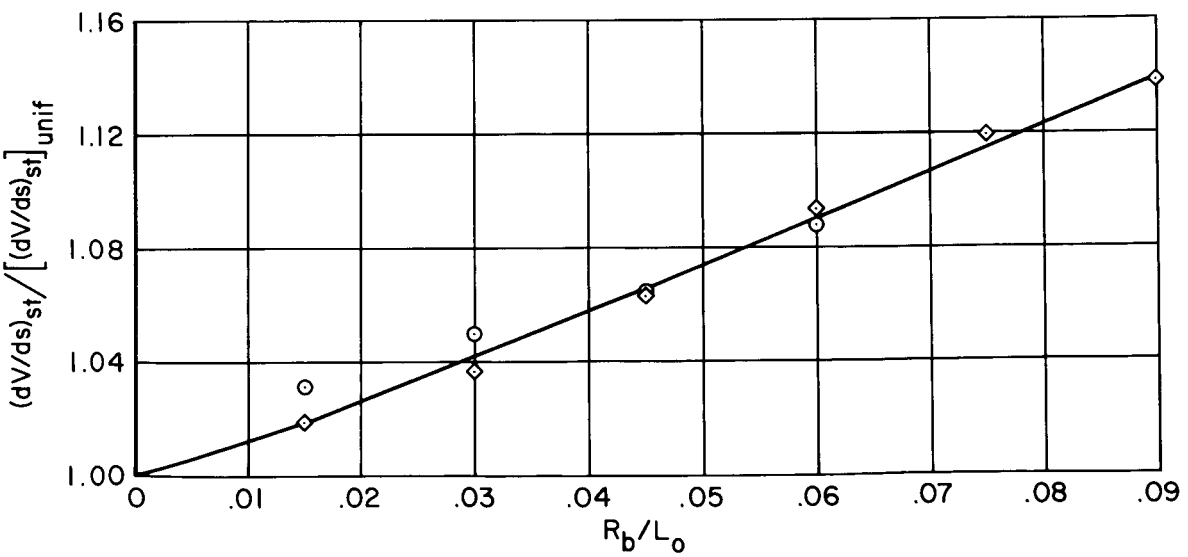

(c) Stagnation-point velocity gradient.

Figure 8.- Ratio of nose radius to shock radius, shock standoff distance, and stagnation-point velocity gradient normalized by uniform flow values for ellipsoidal nose; $B_b = 2.25$, $M_o = 20$.

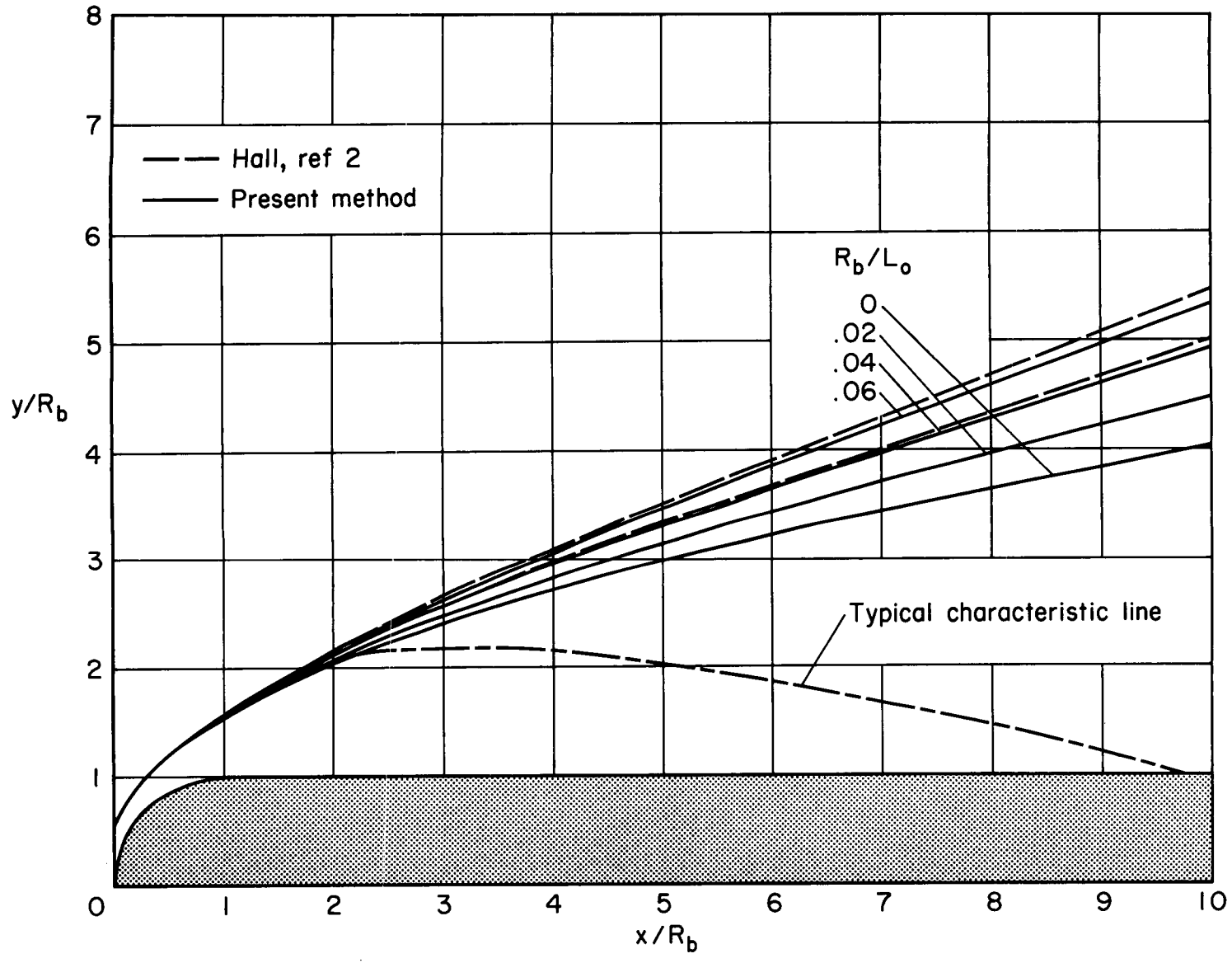

Figure 9.- Shock-wave shape for hemisphere-cylinder; $\gamma = 1.4$, $M_o = 20$.

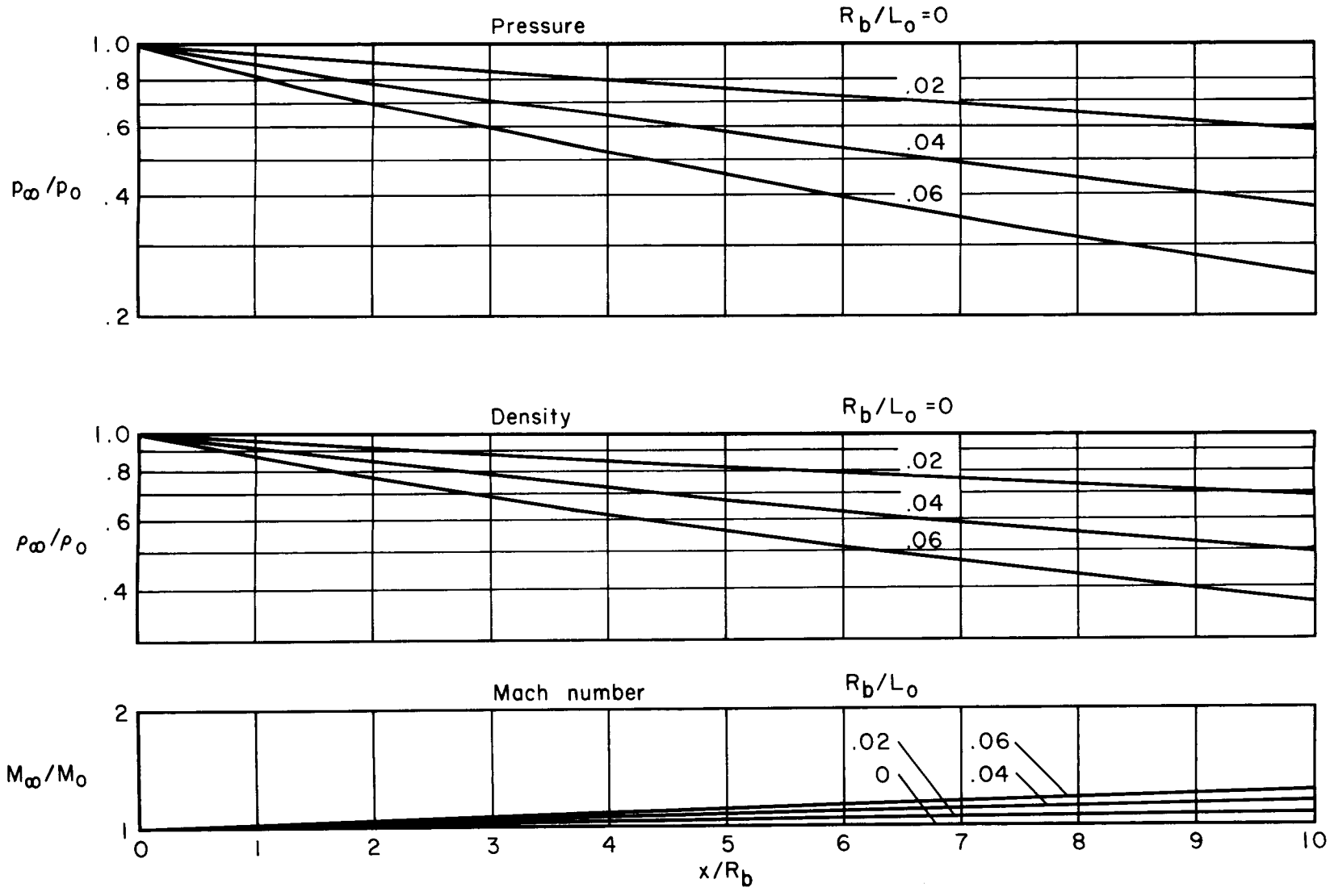

Figure 10.- Variation of free-stream properties upstream of shock wave for a hemisphere-cylinder in a source flow; $\gamma = 1.4$, $M_o = 20$.

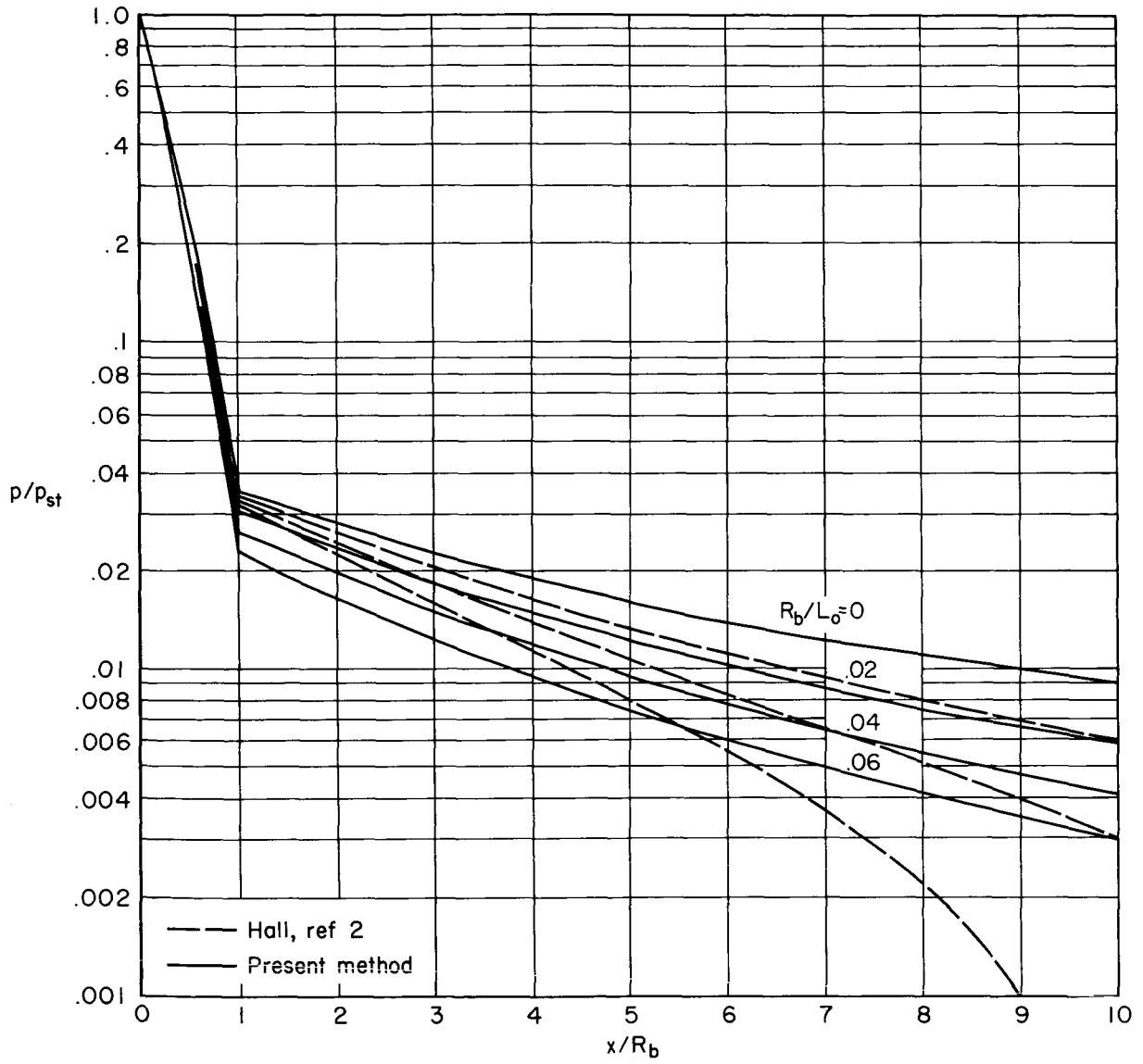

(a) Ratio of local pressure to stagnation-point pressure.

Figure 11.- Pressure distribution along hemisphere-cylinder; $\gamma = 1.4$, $M_o = 20$.

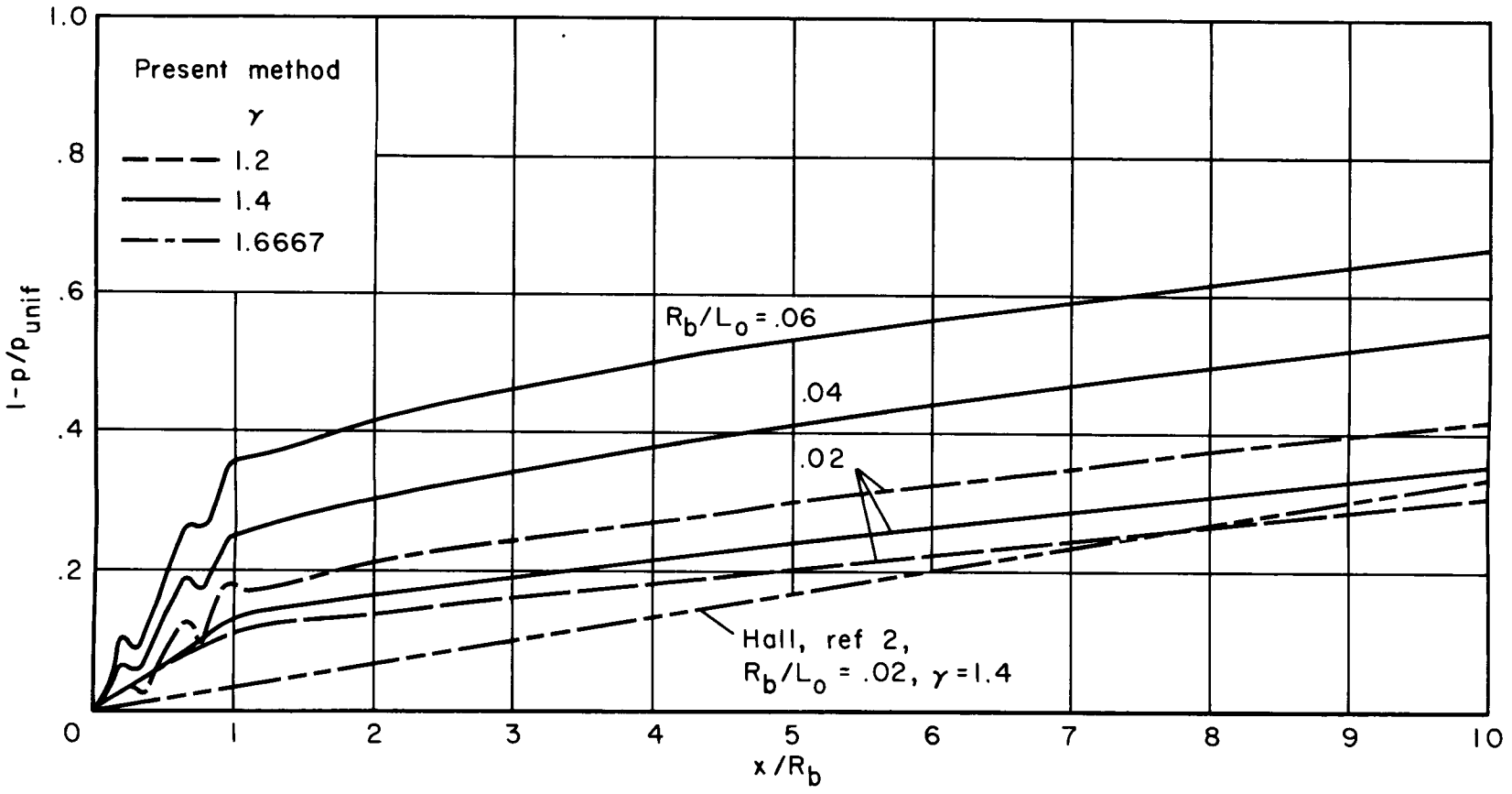

(b) Reduction in surface pressure.

Figure 11.- Concluded.

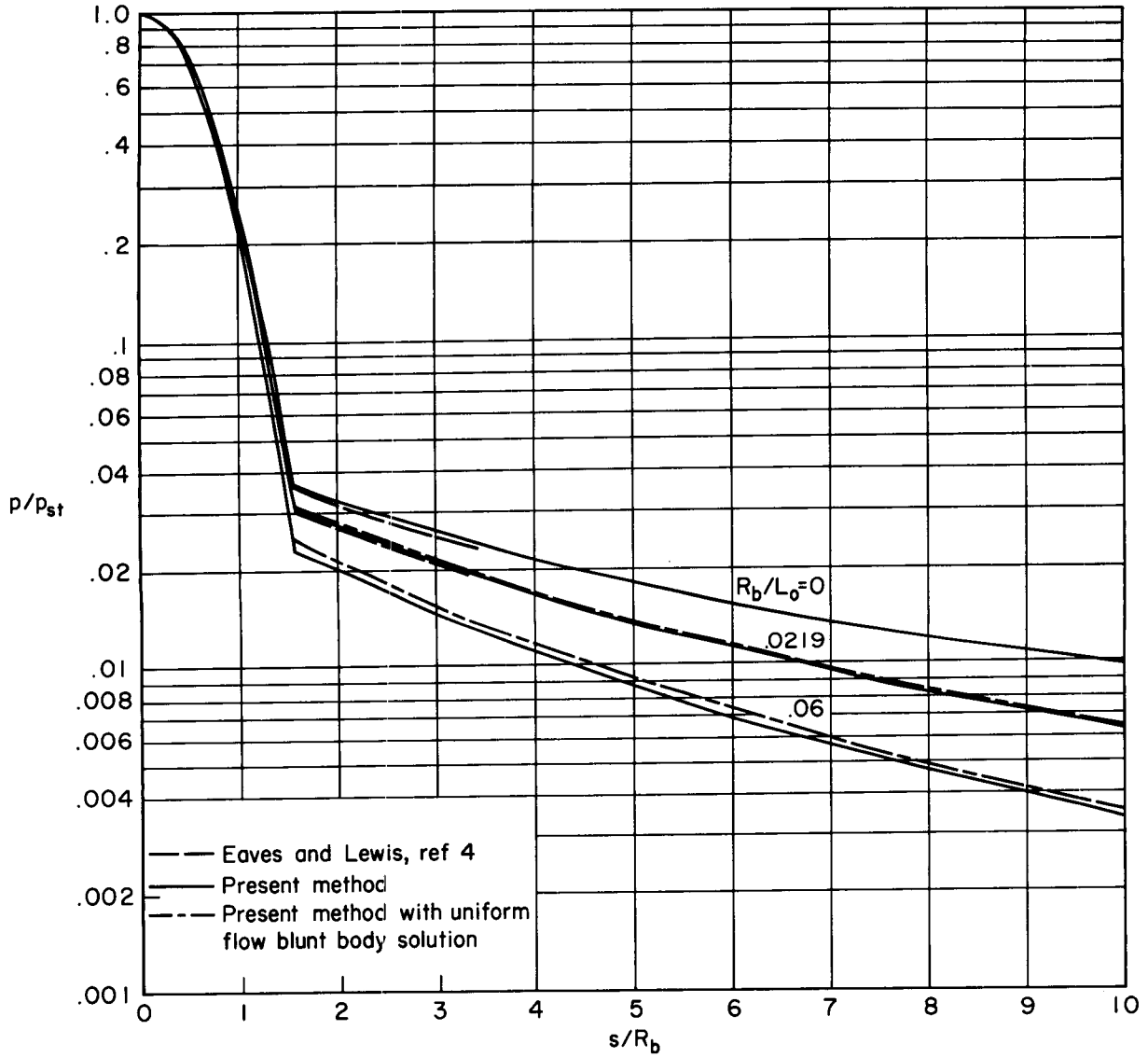

Figure 12.- Comparison of pressure distributions calculated for hemisphere-cylinder; $\gamma = 1.4$, $M_o = 18$.

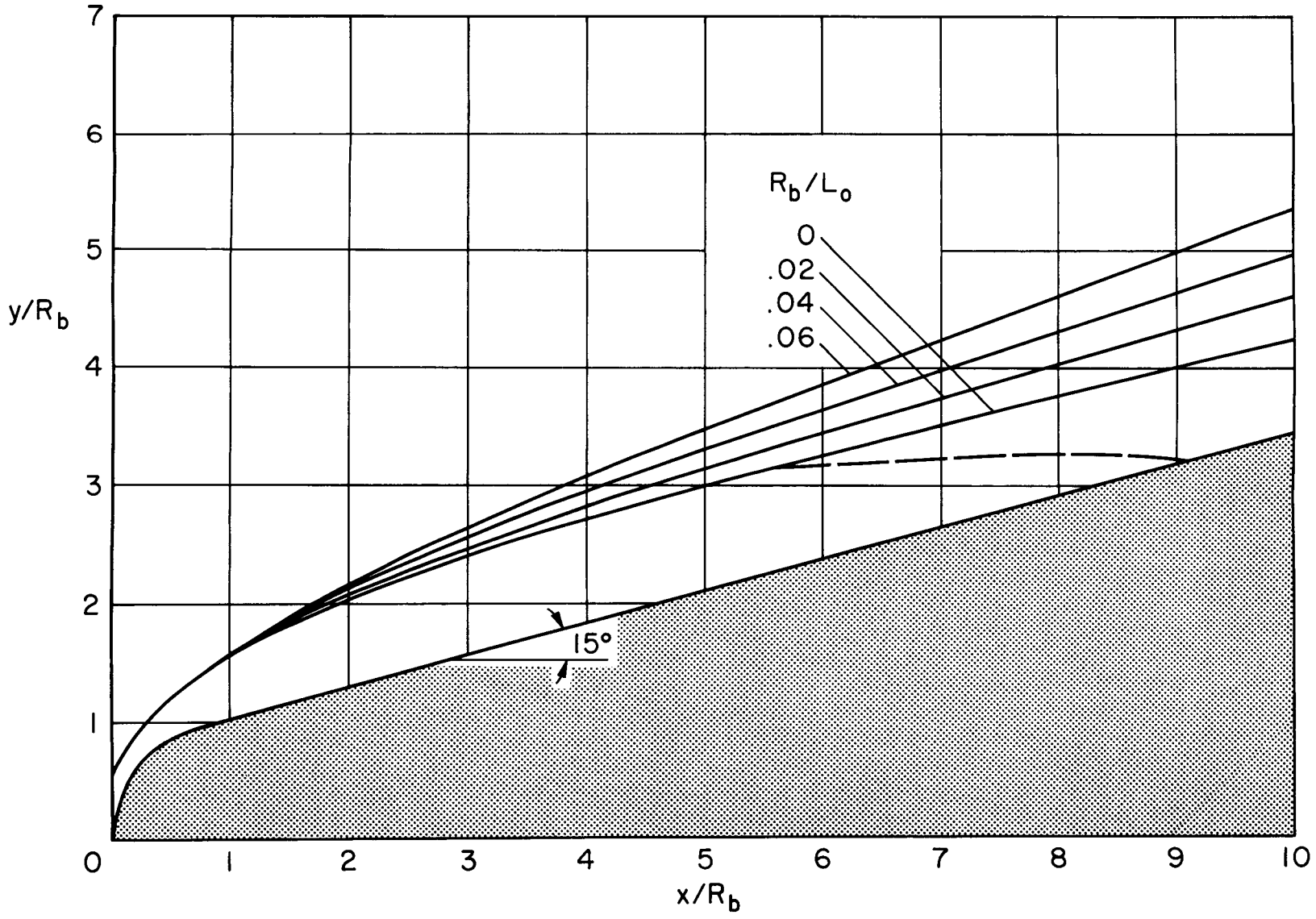

(a) $\theta_c = 15^\circ$

Figure 13.- Shock-wave shape for spherically blunted cone; $\gamma = 1.4$, $M_\infty = 20$.

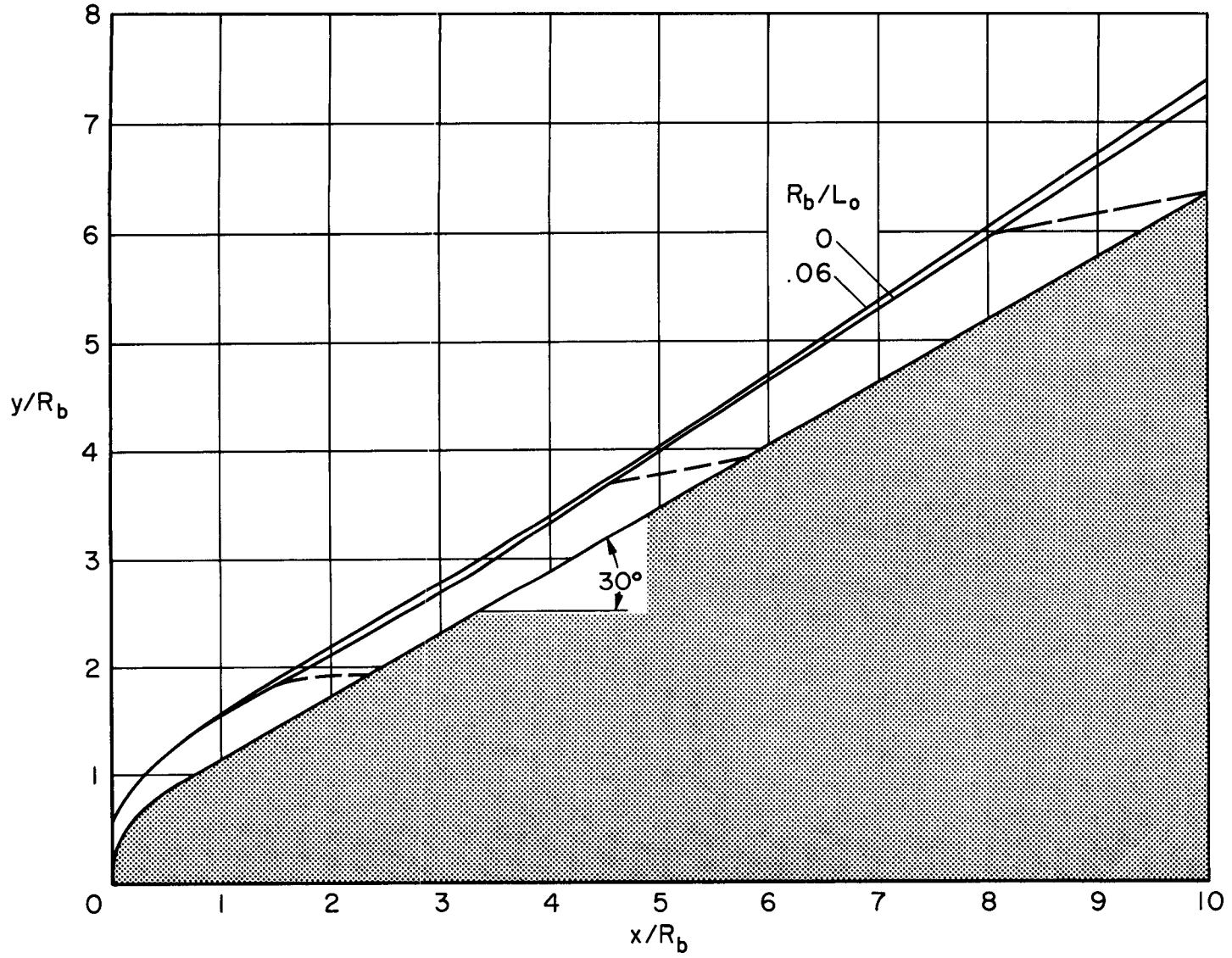

(b) $\theta_c = 30^\circ$

Figure 13.- Concluded.

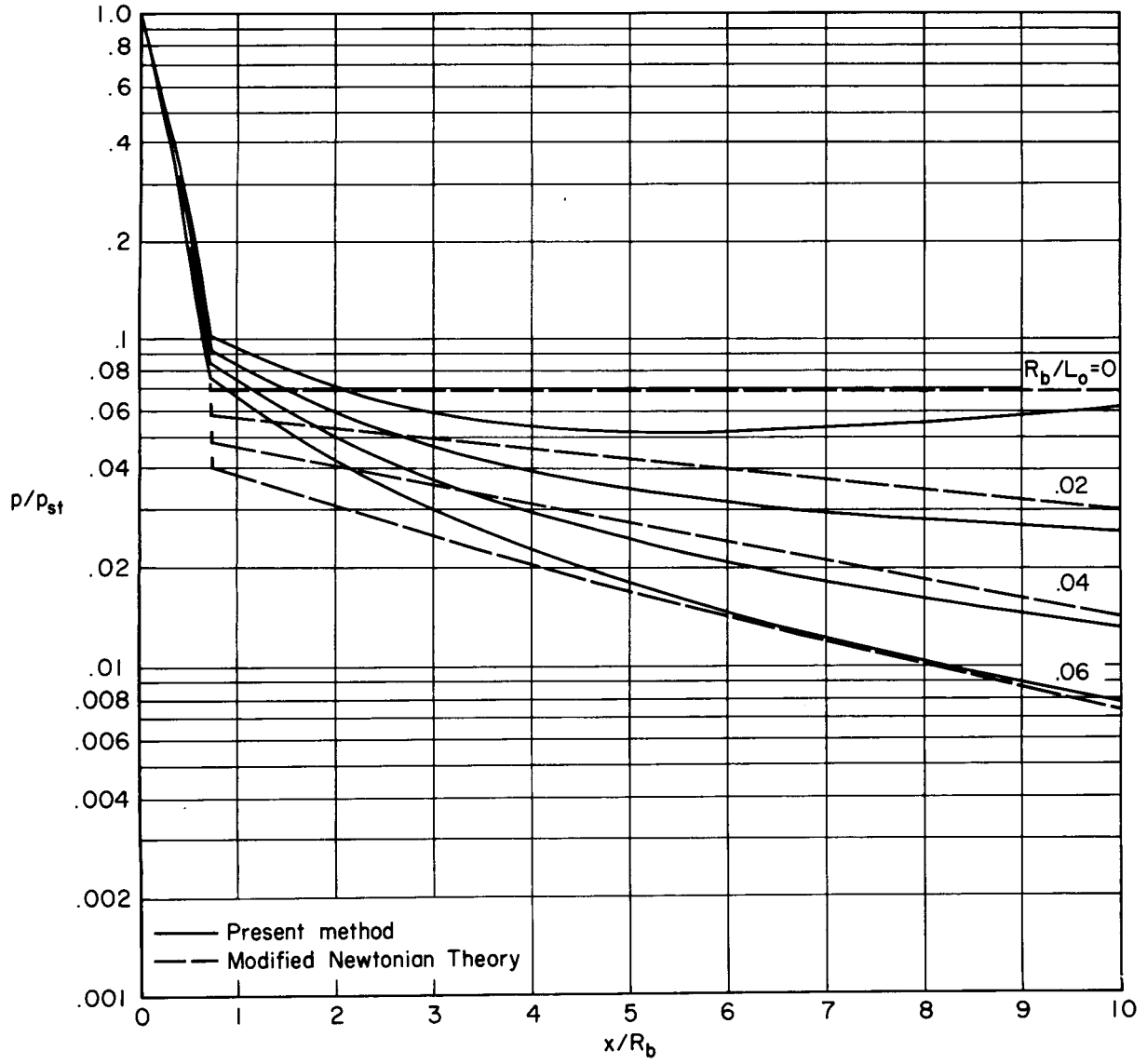

(a) $\theta_c = 15^\circ$

Figure 14.- Pressure distribution along spherically blunted cone; $\gamma = 1.4$, $M_\infty = 20$.

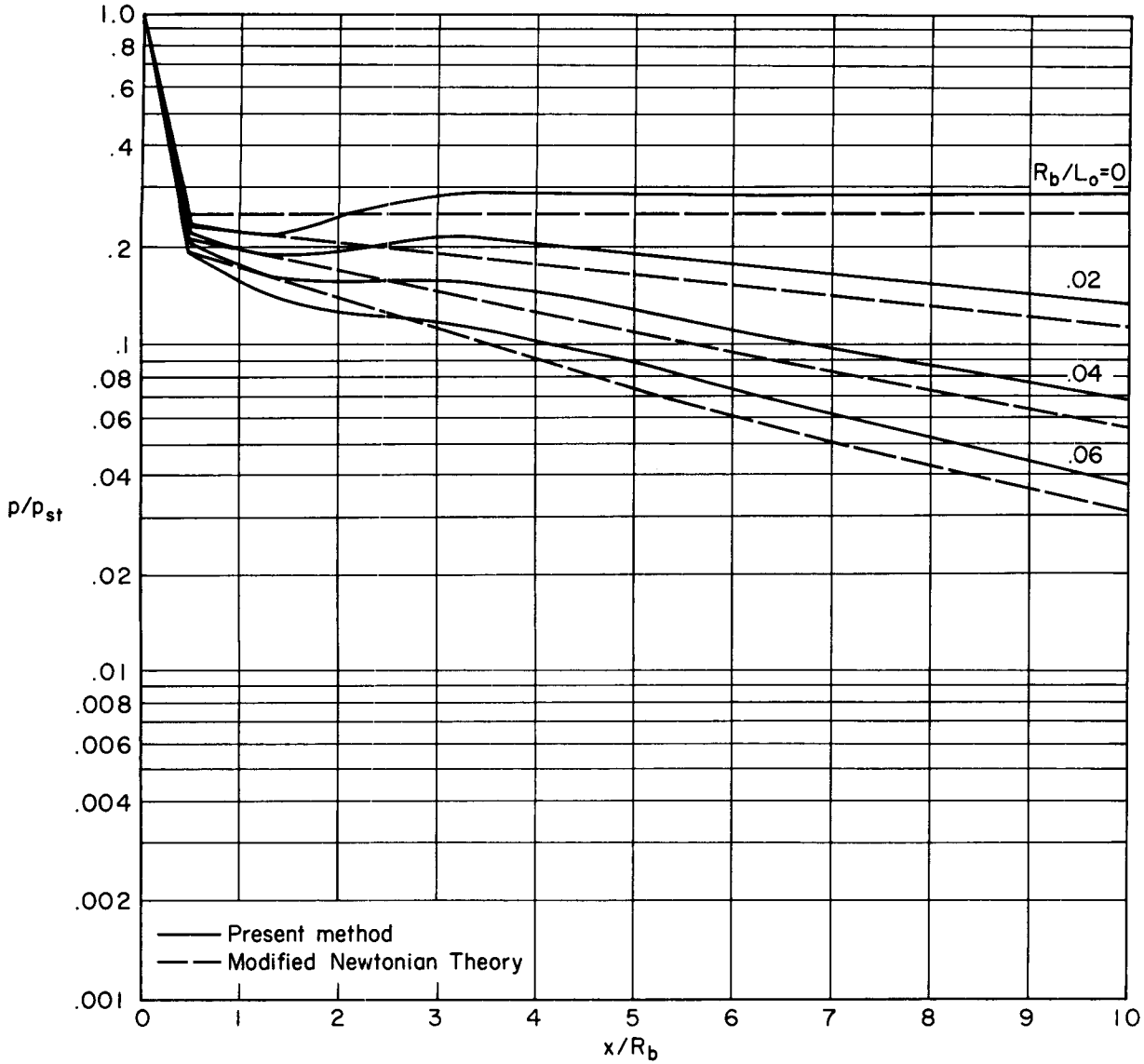

(b) $\theta_c = 30^\circ$

Figure 14.- Concluded.

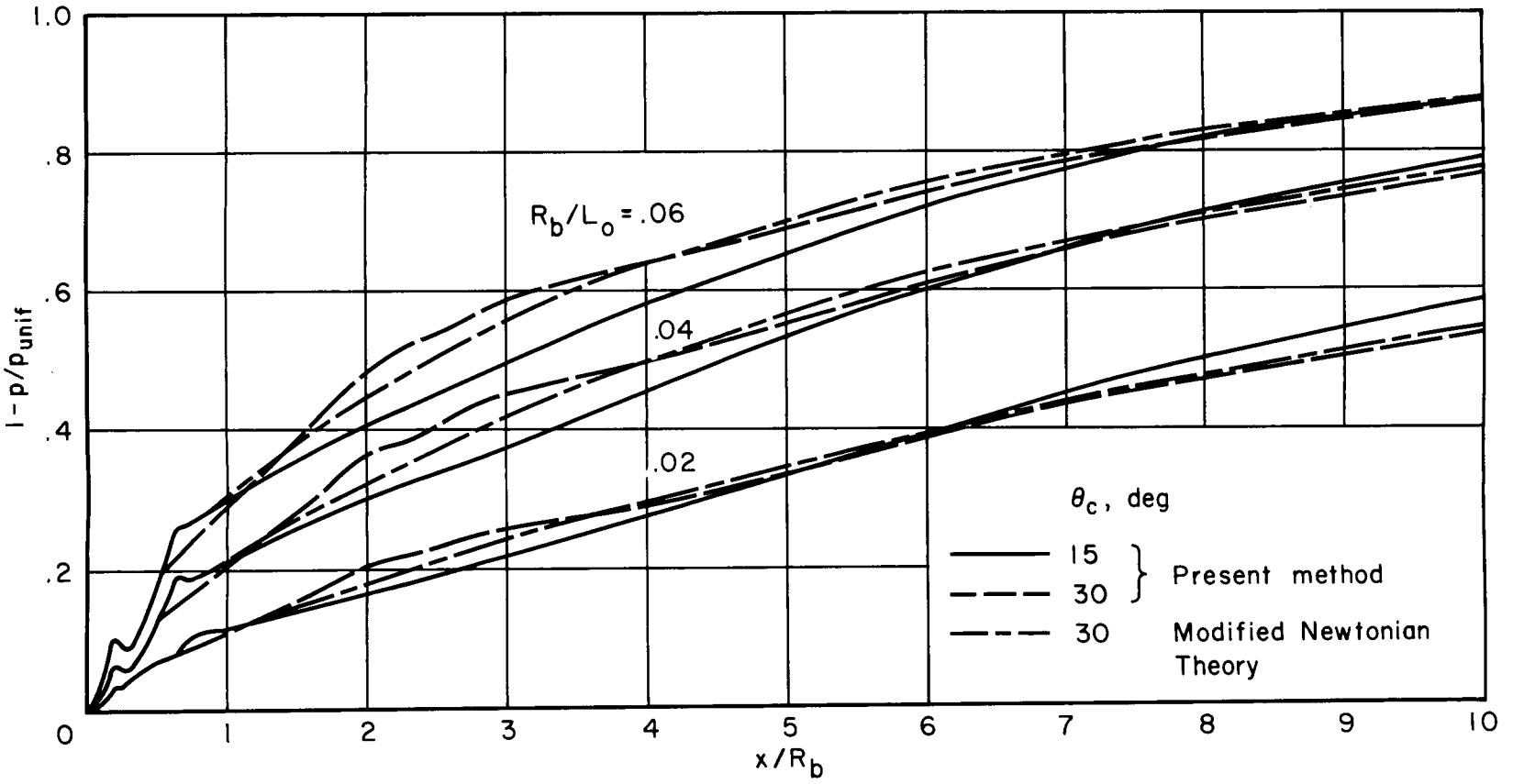

Figure 15.- Reduction of pressure along blunted cones with source flow; $\gamma = 1.4$, $M_o = 20$.

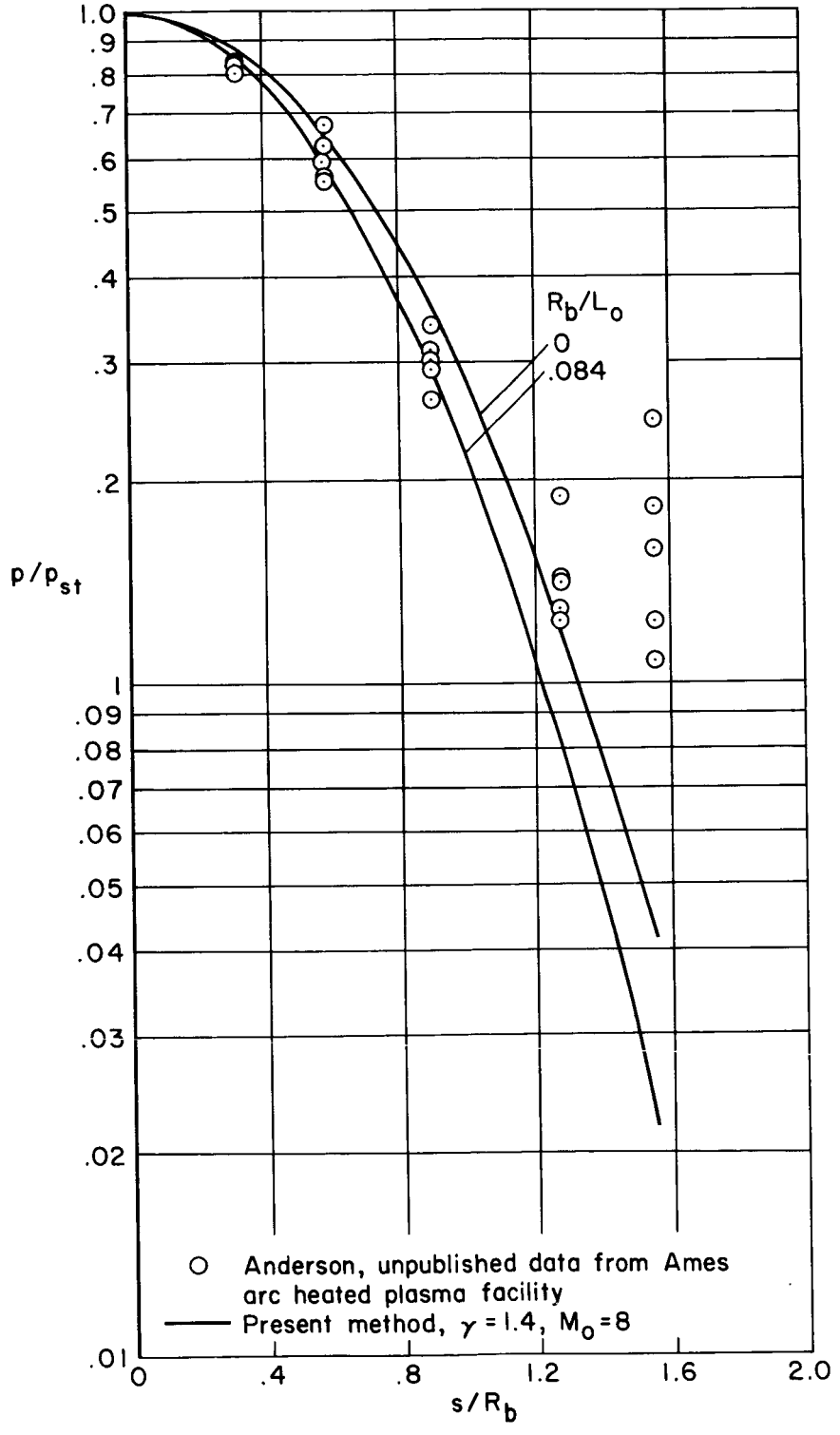

Figure 16.- Pressure distribution on hemisphere in an arc-heated nitrogen stream for stagnation enthalpies from 10 to 20 MJ/kg; R_b = 1.27 cm, L_o = 15.10 cm.

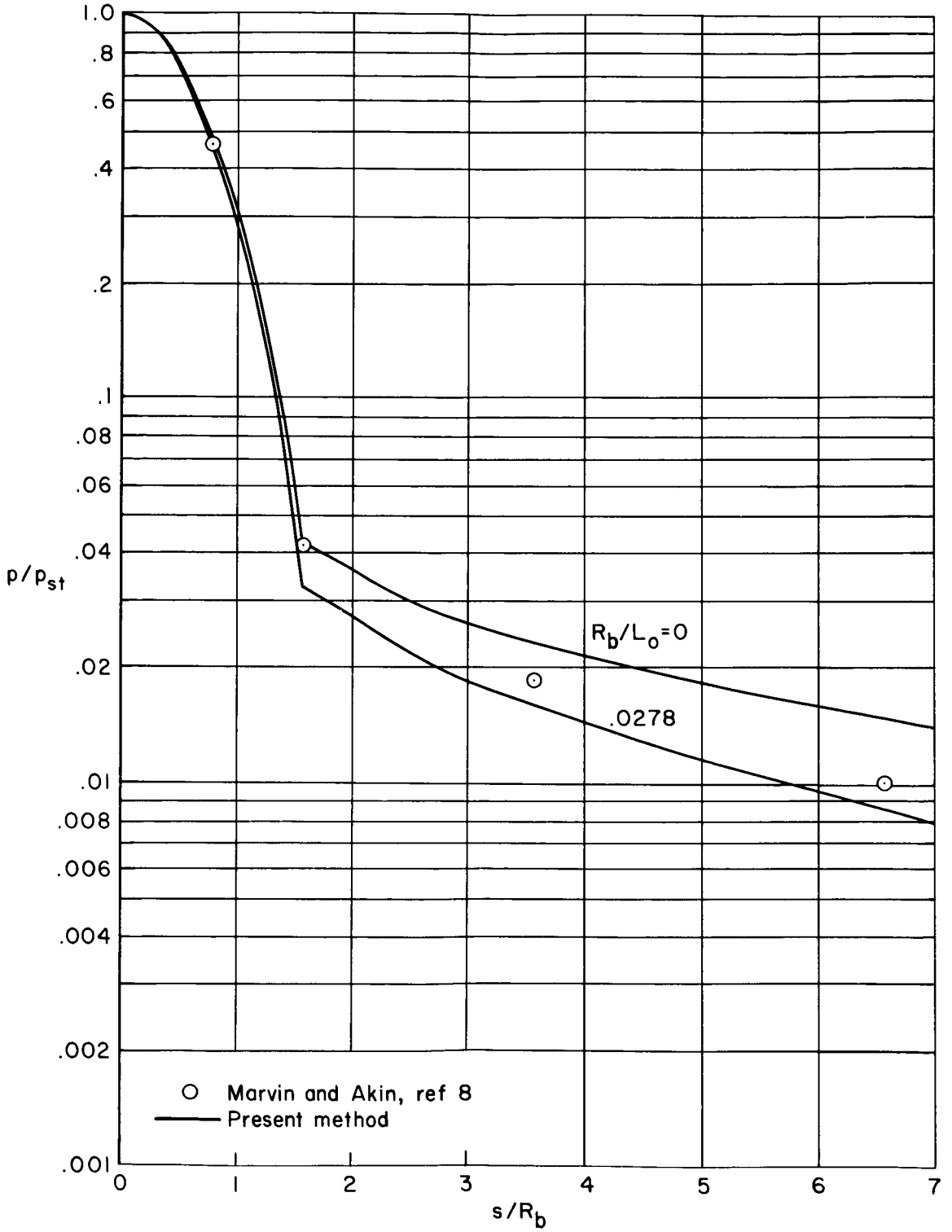

Figure 17.- Pressure distribution along hemisphere cylinder in Ames 1-foot shock tunnel with argon as the test gas; V_o = 3.96 km/s, ρ_o = 0.954 g/m^3, p_o = 0.586 N/m^2, R_b = 2.54 cm, L_o = 91.5 cm.

"The aeronautical and space activities of the United States shall be conducted so as to contribute . . . to the expansion of human knowledge of phenomena in the atmosphere and space. The Administration shall provide for the widest practicable and appropriate dissemination of information concerning its activities and the results thereof."

—NATIONAL AERONAUTICS AND SPACE ACT OF 1958

NASA SCIENTIFIC AND TECHNICAL PUBLICATIONS

TECHNICAL REPORTS: Scientific and technical information considered important, complete, and a lasting contribution to existing knowledge.

TECHNICAL NOTES: Information less broad in scope but nevertheless of importance as a contribution to existing knowledge.

TECHNICAL MEMORANDUMS: Information receiving limited distribution because of preliminary data, security classification, or other reasons.

CONTRACTOR REPORTS: Technical information generated in connection with a NASA contract or grant and released under NASA auspices.

TECHNICAL TRANSLATIONS: Information published in a foreign language considered to merit NASA distribution in English.

TECHNICAL REPRINTS: Information derived from NASA activities and initially published in the form of journal articles.

SPECIAL PUBLICATIONS: Information derived from or of value to NASA activities but not necessarily reporting the results of individual NASA-programmed scientific efforts. Publications include conference proceedings, monographs, data compilations, handbooks, sourcebooks, and special bibliographies.

Details on the availability of these publications may be obtained from:

SCIENTIFIC AND TECHNICAL INFORMATION DIVISION

NATIONAL AERONAUTICS AND SPACE ADMINISTRATION

Washington, D.C. 20546